HYBRID ENERGY MANAGEMENT SYSTEM FOR ELECTRIC VEHICLES

by

Hazem Magdi Sharf

A Thesis presented to the Faculty of the
American University of Sharjah
College of Engineering
In Partial Fulfillment
of the Requirements
for the Degree of

Master of Science in
Electrical Engineering

Sharjah, United Arab Emirates

December 2021

Declaration of Authorship

I, Hazem Magdi Sharf, declare that this thesis is my own work and, to the best of my knowledge and belief, it does not contain material published or written by a third party, except where permission has been obtained and/or appropriately cited through full and accurate referencing.

Signed: Hazem Magdi Sharf

Date: 7th of January, 2022

Approval Signatures

We, the undersigned, approve the Master's Thesis of Hazem Magdi Sharf

Thesis Title: Hybrid Energy Management System For Electric Vehicles

Date of Defense: 28th of November, 2021

Name, Title and Affiliation	Signature
Dr. Mohamed Hassan Professor, Department of Electrical Engineering Thesis Advisor	
Dr. Ahmed Osman Professor, Department of Electrical Engineering Thesis Co-Advisor	
Dr. Mohammad Jaradat Professor, Department of Mechanical Engineering Thesis Committee Member	
Dr. Mostafa Shaaban Associate Professor, Department of Electrical Engineering Thesis Committee Member	
Dr. Oualid Hammi Acting Head Department of Electrical Engineering	
Dr. Lotfi Romdhane Associate Dean for Graduate Affairs and Research College of Engineering	
Dr. Sameer Al-Asheh Interim Dean College of Engineering	
Dr. Mohamed El-Tarhuni Vice Provost for Research and Graduate Studies	

Acknowledgements

I would like to thank my advisors Dr. Mohamed Hassan and Dr. Ahmed Osman for providing knowledge, guidance, and valuable insights throughout my research stages. I am deeply beholden for their great assistance, worthy discussions and suggestions and for their valuable time spent in supervising my work on this thesis. I would also like to thank Ms. Eiman ElGhanam for her support and motivation during the different stages of my work. My gratitude is extended to the professors of the Electrical Engineering department who delivered my Masters level courses with mighty teaching methods and skills. Lastly, I would like to thank AUS for assigning me as graduate assistantship and granting me scholarship and stipend.

Last but not least, my sincerest gratitude goes to my family for their endless support throughout my years of education and beyond.

Dedication

To my family.

Abstract

Boosting the performance of the energy storage system (ESS) of electric vehicles (EV) is of great significance to achieve their pervasion and encourage their mass adoption, which will, in turn, curtail the emission of greenhouse gases and promote a cleaner environment. The objective of this work is to develop and evaluate the capabilities of an EV hybrid energy storage system (HESS) that consists of a main source, namely the Lithium-ion (Li-ion) battery, and an auxiliary source, namely the supercapacitor (SC), to provide more efficient EV energy management. The integration of supercapacitors in EV energy storage systems (ESS) is expected to greatly enhance their performance by addressing high current requirements and extending the EV battery lifetime. Accordingly, this thesis proposes a strategy for managing the energy flow between the integrated battery-supercapacitor HESS and the EV motor to efficiently meet the energy requirements of the EV driving experience. Several simulations are implemented using MATLAB/Simulink to track the current output of each energy source, i.e. the Li-ion battery and the supercapacitor, and their corresponding state-of-charge (SoC). The performance and aging of the HESS operating with the proposed energy management strategy are then evaluated and compared to the performance of traditional ESS without supercapacitors by calculating different stress parameters and aging factors. Additionally, a scaled-down experimental model is developed and tested to validate the simulation results. Performance evaluation of the proposed HESS based on results of the conducted simulations and experiments reveal that the life expectancy of the battery banks is improved by an average of four times, which proves the employment of the SC bank to be cost-effective. Additionally, the remaining energy stored in the EV battery at the end of the driving cycle is higher when the SC bank is used, resulting in increased driving range.

Keywords: supercapacitors; Li-ion battery; electric vehicle; hybrid energy storage system; state-of-charge.

Table of Contents

List of Figures

List of Tables

List of Abbreviations

Ah	Ampere-hour
EV	Electric Vehicle
ESS	Energy Storage System
HESS	Hybrid Energy Storage System
Li-ion	Lithium ion
SC	Supercapacitor
SEI	Solid Electrolyte Interphase
SoC	State-of-Charge

Chapter 1. Introduction

1.1. Introduction

In this chapter, a short introduction is provided to describe, in brief, the problems facing the EV industry that hinder frequent purchases of these automobiles. The need for an efficient EV energy storage and management system is then highlighted to motivate the integration of auxiliary energy storage units, i.e., supercapacitors (SC), with conventional Li-ion battery banks. Accordingly, the problem investigated in this study is presented followed by the thesis objective and contribution. Finally, the general organization of this thesis document is outlined.

1.2. Overview

In times where green energy and a greener environment are sought after, the ubiquity of EVs must be set as a goal to achieve, as it brings about several environmental advantages including the reduction of carbon dioxide gas emission, which is considered as the main cause of global warming [1]. Nevertheless, among the major factors obstructing the prevalence of electric vehicles (EVs) are driving range limitations and EV battery lifetime. The driving range of EVs is limited by the maximum capacity of their energy storage units. Hence, increasing the driving range requires increasing the maximum battery capacity and improving the efficiency of energy storage and provisioning to the EV motor. However, increasing the driving range by enlarging the capacity of the battery bank translates into higher EV prices, since the battery size and capacity are the highest contributors to the cost of EVs. On the other hand, dynamic wireless EV charging (DWC) systems are being developed to enable re-charging the EV battery during the vehicle's motion, thereby extending the EV driving range without the need for larger EV batteries [2][3][4]. Nevertheless, the inherent misalignments during EV mobility cause fluctuations in the charging power, in addition to the variations in received energy at different EV driving velocities [5]. This unstable energy supply impacts the performance and lifetime of the EV battery in contrast to regulated energy from plug-in charging stations, despite the range extension and other advantages offered by DWC systems. Accordingly, improving the efficiency of the EV energy storage system is inevitable to increase the lifetime of the Lithium-ion (Li-ion) battery

packs and reduce the EV operational costs by decreasing the battery replacement frequency [6]. Extensive research is currently being conducted to enhance the energy storage system of EVs and extend the EV battery life through the integration of supercapacitors [7][8], forming a hybrid energy storage system (HESS). The joint operation of the EV battery and SC bank helps reduce the load on the EV battery and addresses the high current and power requirements of the EV motor during different driving cycles. In addition, supercapacitors can be utilized to regulate the energy received from DWC systems. This HESS then enhances the EV driving capabilities and improves the quality of experience (QoE) offered to EV drivers, thereby encouraging large-scale adoption of EVs.

Supercapacitors are electrolytic capacitors that are manufactured differently compared to ordinary capacitors. Ordinary supercapacitors use aluminum sheets as conductors, whereas supercapacitors are designed with carbon films. The construction of SCs allows them to exhibit high values of capacitance and increases their energy density in comparison with ordinary electrolytic capacitors, although it remains lower than that of Li-ion batteries. Nevertheless, supercapacitors offer distinguishable features that complement those of the Li-ion batteries, making the integration of both sources viable and promising. The main distinguishing characteristic of an SC is its high-power density compared to Li-ion batteries, which entails that it can release significantly higher power in a shorter time compared to Li-ion batteries. As highlighted earlier, the efficiency of Li-ion batteries degrades in times of high current demand, leading to high thermal stress that negatively impacts the lifetime of the battery. On the other hand, having a high-power density implies that in times when the current demand by the load is high, this current can be supplied by the supercapacitor. Hence, high current requirements will no longer be addressed by the Li-ion battery, eliminating thermal stress, and prolonging the battery's lifetime. This is expected to tremendously improve EV performance and reduce its operational costs by reducing the degradation rate of the EV battery and hence, reducing the need for replacement. Moreover, an SC exhibits a fast response to electrostatic charge and discharge, because no chemical reactions are involved in its charging and discharging processes, unlike Li-ion batteries. This feature allows the device to be suitable for wireless charging applications as it can capture the received energy faster despite the inherent fluctuations. Another significant feature of

an SC is that its internal resistance is significantly small that it can be neglected; hence, the expected power loss is minimal [7].

1.3. Thesis Objectives

To tackle the problems of EV battery aging and degradation due to high current demands, an auxiliary energy storage source, namely a supercapacitor, is integrated to form a hybrid energy storage system (HESS). To ensure the efficient operation of this HESS, this thesis proposes two energy management strategies to manage the energy flow and exchange between the EV battery and SC bank based on the speed profile of the EV driving cycle. In particular,

1. An energy exchange strategy is proposed to manage the energy supply from the EV battery and the integrated SC bank when the EV is driven in low-speed zones, aiming to eliminate the burden on the battery during frequent stopping and acceleration.
2. A strategy for the joint operation of the battery and SC bank in driving cycles with medium/high speeds is proposed.
3. A controlled power electronic circuit is developed to optimally manage the flow of energy into the EV motor.

The design of the proposed energy management strategies and the corresponding power electronic circuitry are addressed in this thesis aiming to develop a practical HESS that improves the overall EV battery life. The proposed strategies are robust against fluctuations in the EV wireless charging systems.

1.4. Research Contribution

The contributions of this research work can be summarized as follows:

- Proposed efficient and practical strategies/techniques to manage the flow of energy from the main and auxiliary energy sources, during low-speed and high-speed driving terrains, leading to high-performance, more efficient hybrid energy storage system that results in longer mileage and extended battery life.
- Employed an EV battery aging model to evaluate the battery loss in capacity and assess the improvements provided by the supercapacitors.

- Developed an experimental prototype of the HESS to verify the functionality of the proposed strategies.

1.5. Thesis Organization

The rest of this thesis is organized as follows: Chapter 2 provides background information about the modeling and operation of Lithium-ion batteries and supercapacitors, followed by a description of some of the related works on the integration of batteries and supercapacitors in HESS. In Chapter 3, the proposed energy management strategies for low, medium, and high-speed zones are discussed in detail, along with a description of the electronic circuitry used to interconnect the two energy sources. Chapter 4 outlines the simulation and experimental setup for both the traditional ESS battery and the HESS. The results acquired from the simulations and the experimental setup are presented in Chapter 5. Conclusions and future works are then highlighted in Chapter 6.

Chapter 2. Background and Literature Review

In this chapter, the fundamentals of the proposed hybrid energy storage system are discussed. First, a brief discussion of the working mechanisms and aging factors of Li-ion batteries is presented, followed by a description of the modeling and operation of supercapacitors and the DC/DC converter topologies. A detailed literature review of different battery-SC integration strategies is then presented, summarizing state-of-the-art literature on this topic.

2.1 Lithium-ion Batteries

Lithium-ion (Li-ion) batteries are characterized by their large energy density per unit weight. This, combined with their large volume, is why Li-ion batteries have replaced Ni-MH batteries in almost all computers and mobile phone applications. The active developments and recent advancements of EVs are accompanied with notable leaps in battery technology enhancements to be used as energy storage. Particularly, Li-ion batteries have emerged immensely for utilization in EV ESSs, due to their superior performance, reliability, and safety, which enhance the overall performance of EVs. The structure of a Li-ion battery is shown in Figure 2-1.

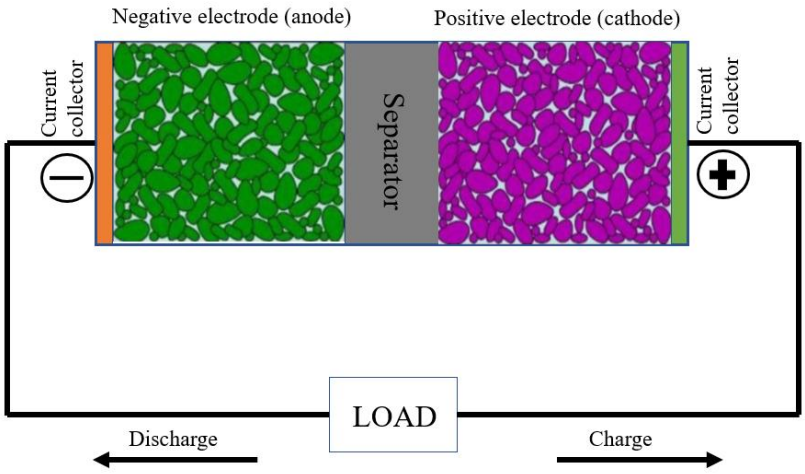

Figure 2-1: Lithium-ion battery structure.

As shown in Figure 2-1, a Li-ion battery generally comprises of a positive electrode of Lithium Cobalt Oxide ($LiCoO_2$), Lithium Manganese Oxide ($LiMnO_2$ or $LiMn_2O_4$) or Lithium Nickel Oxide ($LiNiO_2$), a negative electrode of hard carbon or graphite, an

electrolyte of a non-aqueous solvent comprising ethylene carbonate (EC) or propylene carbonate, and $LiPF_6$ as a supporting electrolyte [9].

2.1.1 Working mechanism

The operation of Li-ion batteries can be described as follows. When the battery is depleted, it means that the Lithium ions have stabilized in their metal oxide form. The charging process of the Li-ion battery forces the Lithium ions to break loose from the metal oxide and move towards the anode through the non-aqueous electrolyte. The non-stable Lithium ions settle on the graphene structure. The battery is fully charged when all the ions move to the other side. On the other hand, the battery discharges when it is connected to the load. The flow of electricity takes place since the electrons pass through the closed circuit, whereas the Lithium ions go back to their stable state through the electrolyte.

2.1.2 Battery degradation

Battery degradation analysis is of critical importance to assess and evaluate the enhancements of any new technology, algorithm or additional components adjoined to the battery. In this case, the supercapacitor bank is employed and the advantages it provides are characterized in terms of the increase in the battery lifetime and driving range.

Battery degradation is quantified by the increase in the battery's internal resistance and capacity fade [10]. As time progresses, the internal resistance rises indicating battery degradation. Additionally, the capacity which is measured in Ampere-hour (Ah) starts fading, which means that the battery is no longer able to supply the same amount of energy as it previously did. An increase in internal resistance and a reduction in capacity occurs due to several mechanisms: the formation and growth of solid electrolyte interphase (SEI) [11] which causes loss of cyclable lithium, loss of active materials, structural changes of the electrodes [12] and lithium plating [13]. These occur due to several stress factors imposed on the battery during operation.

2.1.3 Aging factors

2.1.3.1. Rise in internal resistance

There are many approaches discussed in the literature to quantify the amount of degradation taking place. Quantifying the degradation through the increase in internal resistance is carried out empirically by measuring the internal resistance of the battery for several time intervals in different operating conditions and forming a regression line to evaluate the degradation [14].

2.1.3.2. Capacity fading

Several equations are reported in the literature to calculate the loss in battery capacity. Most of these equations are developed using approximations and linearization techniques that give a good estimate of the loss and remaining capacity.

Usually, aging associated with capacity fading is divided into two types: calendar aging and cycle aging [15][16][17][18][19]. Calendar aging reflects the battery's inherent degradation over time, the rate of which is affected by several parameters such as: temperature and SoC. Calendar aging (L_{cal}) over a period t can therefore be expressed as a function of the average SoC (σ) and the cell temperature (T) [20] as,

$$L_{cal} = f_t(t, \sigma, \mathrm{T}). \tag{1}$$

Cycle aging, on the other hand, is the aging or loss in capacity associated with a full charging and discharging cycle of the battery. Therefore, each cycle can be considered as an independent event (i) and each event is described by the depth-of-discharge (δ) as [20],

$$L_{cyc} = \sum_{i}^{N} n_i f_c(\sigma_i, \delta_i, T_i). \tag{2}$$

Therefore, the total aging can be expressed as the summation of the two expressions in (1) and (2), as [20],

$$f_d(t, \delta, \sigma, T) = f_t(t, \sigma, \mathrm{T}) + \sum_{i}^{N} n_i f_c(\sigma_i, \delta_i, T_i). \tag{3}$$

However, authors in [20] manipulate these expressions for simplicity by extracting the most significant term to evaluate battery's degradation. Typically, calendar aging is considered whenever a new algorithm is implemented or when the driving cycle spans

one full cycle. Cycle aging is calculated in other research scopes, particularly when the battery itself is being assessed and is placed under a long simulation runtime of few years. Therefore, in this thesis, only calendar aging is considered, while cycle aging calculations are not considered.

The calendar aging due to thermal stress is evaluated in [21]. Thermal stress occurs because of the increased temperature when the battery operates at a high-charging/discharging rate, also known as the C-rate. High temperature arises from three dominant thermal factors. First is the joule heating (Q_j), which contributes to most of the temperature rise and is dependent on the equivalent internal resistance of the battery. Second is the polarization heat value (Q_p), which is the energy required for the diffusion and movement of charges in the electrolyte. Last, the reaction heat value (Q_r), which represents the energy released during the exothermic reaction inside the battery [22]. This energy is equivalent to the energy absorbed during charging. The equivalent heat energy released can be calculated as:

$$P = P_J + P_r + P_p = 3.73 \times 10^{-2} Q_1 I_d + 3.60 I_d^2 R_{ed} + 3.6 I_d^2 R_{pd}\,, \tag{4}$$

where Q_1 is the absorbed energy, R_{ed} is the internal equivalent resistance, I_d is discharging current, and R_{pd} is the equivalent polarization resistance. After finding the total released energy, the total rise in the temperature can be computed using the specific heat capacity (C_p) equation as follows:

$$Q = mC_p\Delta T. \tag{5}$$

Then, the following equation is used to quantify battery's aging:

$$C_{loss} = (a.T^2 + b.T + c)\mathrm{e}^{\left((d.T+e)*C_{rate}\right)} A_{th}, \tag{6}$$

*w*here C_{loss} is the percentage of loss in capacity, T is the battery temperature, C_{rate} is the battery charging and discharging rates, which are measurements of the charge and discharge currents with respect to its nominal capacity. The coefficients a, b, c, d and e are constants and A_{th} is the amount of electricity output by the battery during the cycle (in Ah).

In contrast, the calendar aging associated with the change in SoC is calculated by the authors in [23] as follows:

$$\frac{1}{C_n}\frac{dC_a}{dt} = \left|\frac{dS}{dt}\right| a_p, \tag{7}$$

where a_p denotes a negative degradation constant, S represents the state of charge (SoC) in percentage, C_n represents the ideal capacity of the battery, and C_a is the available capacity of the battery.

2.2. Supercapacitors

Supercapacitors are energy storage devices that store electrical energy electrostatically on porous electrodes typically made from carbon. Because they store charge electrostatically, supercapacitors have higher power densities, reduced temperature dependence, reduced degradation, yet lower energy densities compared to Li-ion batteries. The typical construction of a supercapacitor is similar to that of batteries and is shown in Figure 2-2 with two porous electrodes separated by an electrically insulating separator. Flowing through the device is an aqueous ionic electrolyte carrying charge [24]. Current is transferred to and from the system via current collectors. Supercapacitors have higher energy densities than standard dielectric capacitors since their capacitance reaches as high as 800 Farads.

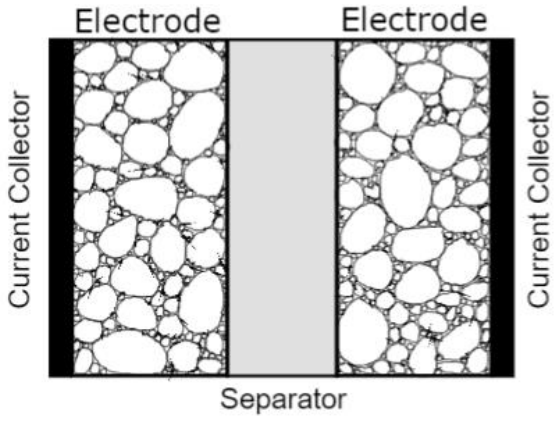

Figure 2-2: Structure of a supercapacitor [24].

Several equivalent circuits are proposed in the literature to model the behavior of supercapacitors. For example, the electrical model of a supercapacitor in [25] shows that the positive and negative electrodes are composed of two RC series network,

collector resistances R_{CP} and R_{CN}, and a separator resistance, R_{SP}. Additionally, in [26] and [27], different models that represent both static and dynamic behavior of supercapacitors are proposed. In [28] and [29], supercapacitors are modeled to illustrate the time domain response, i.e., depending on the time response of the electrical components, which are resistors and capacitors. Moreover, modeling based on the electrochemical and thermal equations to describe their inner behavior is proposed in [30] and [31]. In [32], a study based on fractional orders is conducted to model supercapacitor. Nevertheless, since the main focus of this thesis is to propose an energy management strategy that incorporates supercapacitors to investigate the improvements on the overall system, it is sufficient to understand the working mechanism of this device and the different circuit representations as it helps to comprehend how this device can benefit the system.

2.3. DC/DC Converters

DC/DC converters are the intermediate stage between the main and auxiliary power sources on one hand, and the EV motor on the other hand. They play a vital role in energy transfer, boost and buck the voltages given the charging/discharging situations. Figure 2-3 shows a sample DC/DC converter. The main flaw with this design is that the component parameter such as capacitance and inductance is designed based on the supply voltage and other factors that deemed to be fixed at a certain value during the operation. The supply voltage of the SC bank is continuously varied in this case and therefore this topology cannot be used.

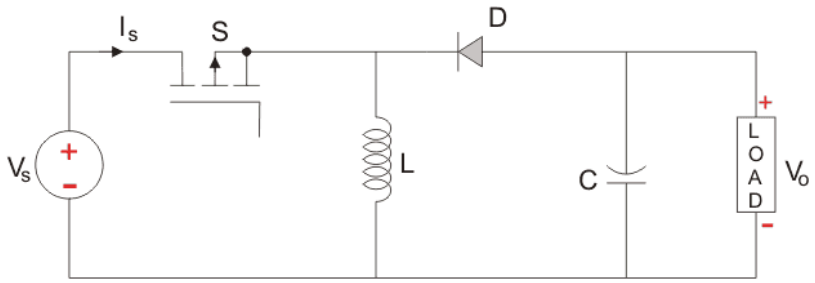

Figure 2-3: A buck-boost DC/DC converter topology.

Different supercapacitor interconnectivity solutions are proposed in the literature, in which DC/DC converters are altered to increase efficiency and improve voltage limitations of the system.

One battery-SC connection configuration known as passive paralleling is proposed in [33], as shown in Figure 2-4. This is the simplest method of combining both energy sources, battery and SC banks in one circuit because the hybridization is formed without any power electronic circuits. This comes with a major disadvantage, as it does not effectively utilize the stored energy of supercapacitor, as it depletes much faster compared to the battery.

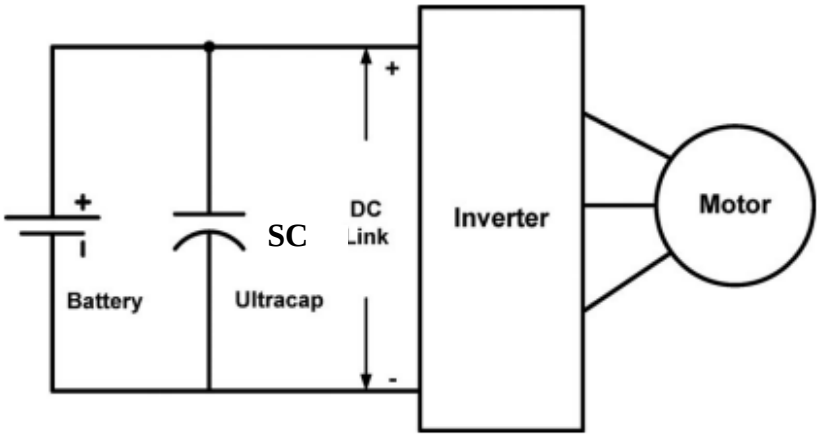

Figure 2-4: Basic passive parallel hybrid configuration [33].

The configuration presented in [34] is the most studied and researched configuration of the HESS. This is because by interfacing the supercapacitor with DC/DC converter, the voltage of the SC can be varied and used in a wide range as it can be controlled by controlling the duty cycle. However, in this topology, the battery bank is directly connected to DC bus and its voltage cannot be varied. This is shown in Figure 2-5.

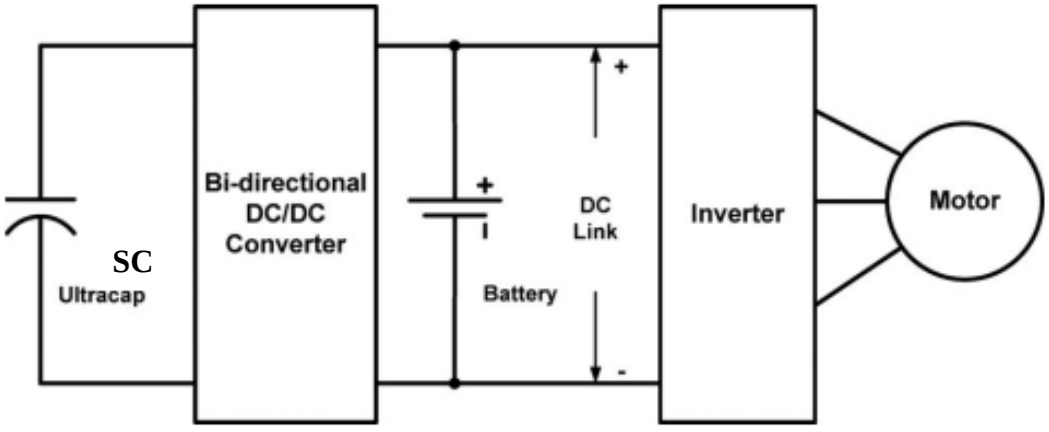

Figure 2-5: Circuit topology with battery connected to DC bus and SC is interfaced with DC/DC converter [34].

The topology presented in [35], shown in Figure 2-6, swaps the position of the energy sources in the configuration discussed in [34]. In this configuration, the voltage of the battery can be maintained lower or higher than the SC voltage. However, the SC voltage level must be tracked and maintained at certain range.

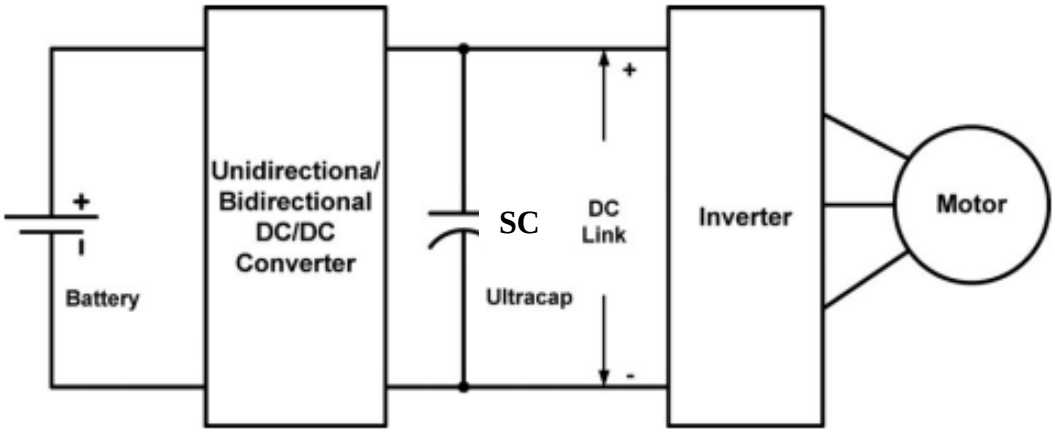

Figure 2-6: Circuit topology with SC connected to DC bus and battery is interfaced with DC/DC converter [35].

The work in [36] compares the two different connections discussed in [34] and [35], to decide whether the battery or the SC should be connected to the DC bus through the DC/DC converters. In their assessment, the authors reveal that connecting the SC to the DC link through a DC/DC converter is better as the large peak current is provided by the SC, which is the main purpose of this electrical component. However, both processes hinder the energy harvesting process from regenerative braking.

The authors in [37] assert that the optimal connection should have both sources connected to the DC bus through a DC/DC converter to have a full control over the energy flow, as shown in Figure 2-7. More issues are also faced in the design of the DC/DC converters. This design allows regenerative braking to occur for both sources and gain full control over the energy flow in the system. This, however, comes with a disadvantage compared to the design proposed in the previous paper because an additional DC/DC converter implies power loss; hence, decreases the achieved efficiency.

The work in [38] compares the topology discussed in [33] with two improved topologies, namely: a three-level converter and a half-controlled converter. The two

topologies aim to reduce the size of the power interface and improve efficiency. However, with extra added switches to the circuit, three-level converter and a half-controlled converter require extra gating signals and increases complexity. Yet, the problem of direct connection of the battery to the DC bus is still faced.

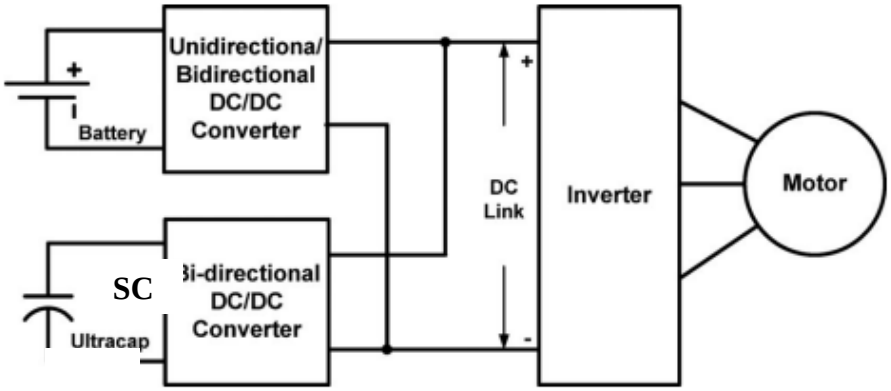

Figure 2-7: Circuit topology with each source interfaced with DC/DC converter allowing variations for both sources [37].

Cao and Emadi [39] proposed a configuration where the low-voltage side is held by the battery pack and is interfaced by a power diode with the DC link held by the supercapacitor bank. This is shown in Figure 2-8. With this topology, a battery bank is expected with lower voltage than the SC to keep the diode reverse biased. However, the voltage level of SC decreases rapidly compared to the Li-ion battery resulting in a forward biased diode, which splits the battery's output current to both the motor and capacitor to charge it. Additionally, connecting the SC directly to the DC bus requires keeping track of its voltage level and maintaining it at certain range.

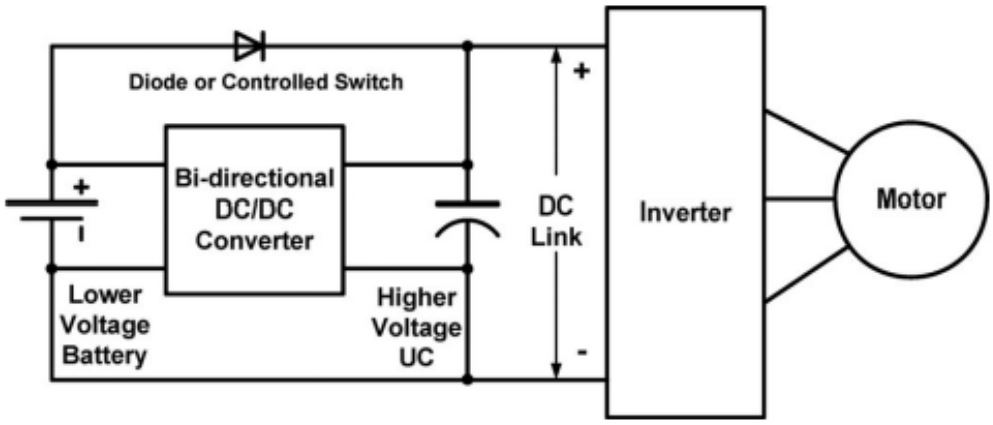

Figure 2-8: A battery-SC connection topology proposed by Cao and Emadi [39].

In [40], the authors state that the usage of DC/DC converters in to integrate SC in ESS must be avoided as it produces instability to the system and suggests a dynamic limitation method to replace it; however, this proposed work is not validated using experimental methods and therefore could be unreliable.

2.4. Battery-Supercapacitor Energy Management Strategies

The challenge encountered when integrating SC with the battery bank lies in developing an energy management strategy to decide when to activate each source for optimal usage of energy. This is where creativity is mandated when facing such a challenge. Therefore, a key goal is to utilize different engineering tools and logic to formulate a strategy that is efficient in handling the energy flow. There are several proposed energy management strategies in the literature aiming for optimal usage of energy sources while taking into consideration what each source is capable of, to benefit the system as a whole. For example, as mentioned previously, SCs have high power density with reduced dependence on temperature. Therefore, they can be used for high current demand. However, SCs have low energy density such that their output current should be optimized to prevent quick depletion. Four different methods are used to accomplish a successful integration of both sources, namely:

- Rule-based (RB) control.
- Optimization-based control.
- Pattern-recognition based control.
- Traffic -based control.

Each of these methods is further described as follows.

2.4.1 Rule-based (RB) control

Rule-based (RB) control is a control method based on heuristic human expertise, through empirical knowledge drawn from domain experts, or sometimes, intuition. The control method is usually formed by complete understanding of the problem followed by lying a set of rules to help achieve a certain objective. RB control can be further broken down into two different categories. First, a deterministic RB method, which is usually based on “if-else” paradigm. Second, fuzzy control that is also “if-else” formatted but with given probabilities.

2.4.1.1 Optimizing for efficiency or battery life in a battery/supercapacitor electric vehicle [41]

In [41], Carter et al. proposed a method by setting a threshold such that if the current demand exceeds that threshold, the SC aids by filling up the excess required power. The major flaw of this approach is its dependence on the driving cycle, as this threshold can be exceeded for a long time resulting in constant energy flow from the supercapacitor which has a fast depletion rate.

2.4.1.2 An adaptive power-split strategy for battery–supercapacitor powertrain—design, simulation, and experiment [42]

In [42], [43], [44] and [45], the same RB method is considered, by applying a low-pass filter to load demand, then extracting the low frequency spectrum of the demand to source it from the battery. The high frequency component is then supplied by the SC. These methods work relatively good in simulation environments. However, different driving cycles require different cut-off frequencies, and it is not practical to adjust it regularly in real life. Also, designing an accurate circuit to achieve the separation of frequencies is a hurdle.

2.4.1.3 Particle swarm optimization for energy management fuzzy controller design in dual-source electric vehicle [46]

In fuzzy logic-based strategies, a weight is allocated for each parameter signifying its importance. Fuzzy logic is introduced in [46] and [47]. The method basically works by feeding several parameters to the processor, such as SoC, desired load and various constraints, and accordingly power split is achieved. The issue with this method is that it requires setting up a big look-up table for the computations before running the algorithm. This in turn imposes longer computation times by the processor. Also, the processor may crash if a specific condition arose during the driving cycle that the designer did not take into consideration.

2.4.1.4 A new strategy for battery and supercapacitor energy management for an urban electric vehicle [37]

Similar to the approach in [46], the authors in [37] propose a fuzzy logic-based method, but with deterministic assignments of the battery and SC instead of assigning weights to different parameters. Similarly, having big flow chart with several branches might

be a problem since frequent computations are deemed necessary as the load fluctuates rapidly and unpredictably.

2.4.1.5 Control of a battery/supercapacitor hybrid energy storage system for electric vehicles [48]

This study considers control theory, particularly model predictive control (MPC), to control the power flow of the two sources in the HESS. The aim of the designed controller is to track the speed of the vehicle and assign the energy distribution among the two sources. However, this approach increases the complexity of the system and does not work with random and unknown terrains.

2.4.2 Optimization-based control

Optimization is a powerful engineering tool that is commonly used to solve complex engineering problems [49]. Optimization in general is a tool that helps find the maxima or minima of an objective, formulated as an objective function, while subjecting the variables to several constraints designed according to the problem. Researchers utilize this control scheme to model HESS and find the set of Pareto optimal points describing the optimal operation of the energy sources accordingly. Optimization-based control can be divided into two categories: global optimization and real-time optimization, where global optimization requires knowledge of the driving cycle, and hence is only suitable for prescheduled routes. Real-time optimization, on the other hand, does not require prior information about the driving cycle, and uses real-time EV driving data to optimize the joint operation of the battery and the SC bank, but the flaws are embodied in the time taken to process and calculate the optimal values which is discussed in [50].

2.4.2.1 Effectiveness of supercapacitors in pure electric vehicles using a hybrid metaheuristic approach [50]

This paper suggests a metaheuristic approach for the operation of the HESS. This approach involves assigning both short-term and long-term plans for a given interval of time and then executing these plans by a controller. The obtained results show notable improvements although the approach has downfalls in the time taken for each time the controller must evaluate the objective function and settle on a plan.

2.4.2.2 Advanced design approach of power split device of plug-in hybrid electric vehicles using dynamic programming [51]

In [51], Li and Kar designed an analytical and a numerical model to optimally design a power split algorithm for the urban dynamometer driving schedule (UDDS) cycle to compute the best power split strategy. This method is, however, not very practical as it works only with one particular driving cycle with a given set of load conditions. In [52] and [53], a complex non-linear optimization problem is formulated for power splitting and is solved via genetic algorithm. Using genetic algorithm means that the problem is treated as a black box making it difficult to understand or track what happens inside. Additionally, using the genetic algorithm can be very time consuming.

2.4.3 Pattern-recognition based control

The two previously mentioned control methods are mostly focused on the power supply side of the system. In other words, the current/voltage profiles are tracked, and the corresponding energy flow algorithm acts accordingly. In this control method, AI is employed to set an eye on the intrinsically unpredictable load fluctuations.

Shen and Khaligh [54] and Moreno et al. [55] used cutting-edge technologies such as machine learning and supervised learning for the purpose of training neural networks to generate output variables that control power split objective.

Using AI for the purpose of power splitting requires the reduction of the dimension of extracted data into a meaningful size. A technique called support vector machine (SVM) is introduced by Liang et al. [56] with which the authors produced four different driving patterns using 18 variables as inputs. Another method called learning vector quantization network is applied to driving pattern classification in [57]. Monte Carlo approach is used in [58] to identify useful features of some given dataset of load profiles.

2.4.4 Traffic -based control

In this method, the control algorithm is not only fed by past and present values, but mainly with future probable incidences. Although this method is not typically utilized in the literature for incorporating SC in ESS, it is indeed a futuristic method that can be beneficial if used with appropriate tools and equipment.

This method requires a real-time GPS data processing operation to be performed at all times, with constant data feeding into the system to locate traffic jams, traffic lights and any hurdles the driver may encounter during the driving cycle. Judgements can be inferred from the given traffic situation including whether the car will be braking or accelerating, and the system will act in accordance. Gong et al. [59] took advantage of a modern governmental intelligent transportation system to log a series of data from traffic flow sensors installed along the freeways by Wisconsin Department of Transport. The major disadvantage of this method is that it requires an entire traffic monitoring infrastructure with reliable communication networks. This requires a large volume of resources and is very costly to build.

Chapter 3. Methodology

This chapter is organized as follows: first, the problem of integrating supercapacitor in EV energy storage system is described and formulated. Then, the method considered to size the supercapacitor bank is illustrated. This is followed by a detailed description of the strategy developed to handle and manage the energy flow. Lastly, the design of DC/DC converters is explained.

3.1. Problem Formulation

The problem at hand is how to integrate a SC bank and utilize it for high current requirements in the EV ESS. This requires an energy management strategy to split the power supply from the two storage devices, i.e., the battery and the SC, for efficient and optimum usage of the energy stored, with the ultimate objective of increasing the EV battery lifetime and the EV driving range. Therefore, the problem can be divided into 3 sub-problems. First, designing and sizing the supercapacitor bank such that the weight, volume, and capacity of the bank are taken into consideration. Second, developing a strategy to manage energy flow and power split of both energy storage elements. Third, designing a circuit with proper DC/DC converter configuration to achieve the desired objectives.

3.2. Sizing of Supercapacitor Bank – Optimization

Before starting to create control methods or designing the corresponding circuitry, the size of the supercapacitor being installed should be considered. Similar to battery banks, SC can be arranged in series and parallel configurations to optimize the total resistance, total output voltage and current. In this work, a non-linear multi-objective optimization problem is designed to maximize the energy that can be stored in the power bank and minimize the size of the bank while adhering to some constraints, such as: weight, volume, and total capacitance. A metaheuristic genetic algorithm is used to run the problem and search for optimal size of the bank. The optimization problem is described as follows:

$$\max \ f_1 = 0.5(v_{SC} n_s)^2 C_{SC} \frac{n_p}{n_s}, \tag{8}$$

$$\min \ f_2 = n_s n_p, \tag{9}$$

such that,

$$C_{sc}\frac{n_p}{n_s} \leq 50, \tag{10}$$

$$m_{SC}n_s n_p \leq 43.75, \tag{11}$$

$$V_{SC}n_s n_p \leq 0.028, \tag{12}$$

$$1 \leq n_s \leq 100, \tag{13}$$

$$1 \leq n_p \leq inf. \tag{14}$$

where, C_{sc} is the capacitance per SC, v_{SC} is the rated voltage per SC, m_{SC} and V_{SC} are the mass and volume per supercapacitor respectively. The specifications of each SC cell are summarized in Table 3-1: Supercapacitor cell specifications.Table 3-1.

Table 3-1: Supercapacitor cell specifications.

Specifications per SC cell	**Value**
Mass (kg)	0.05
Volume (m^3)	42e-6
Voltage (V)	2.7
Capacitance (F)	500

The variable n_s represents the number of SC to be connected in series, whereas n_p represents the number of parallel SC connections. Multiplying the two variables is equal to the total number of SC in the bank.

The first objective function, f_1, maximizes the stored energy while the second function, f_2, minimizes the number of SCs. The constraints are designed such that 7% of the battery is replaced by the SC. Therefore, the added bank will not impose a new weight or space problems. The battery bank of Tesla EVs is reported to weigh 625 kg and occupies 0.4 m^3 volume; therefore, 7% is equivalent to 43.75 kg and 0.028 m^3. The first constraint in (10) addresses the capacitance while the second, in (11), addresses the weight and the third, in (12), is for occupied volume. The pareto front of the multi-objective optimization function is shown in Figure 3-1, and the specifications of the resulting capacitor bank are summarized in Table 3-2.

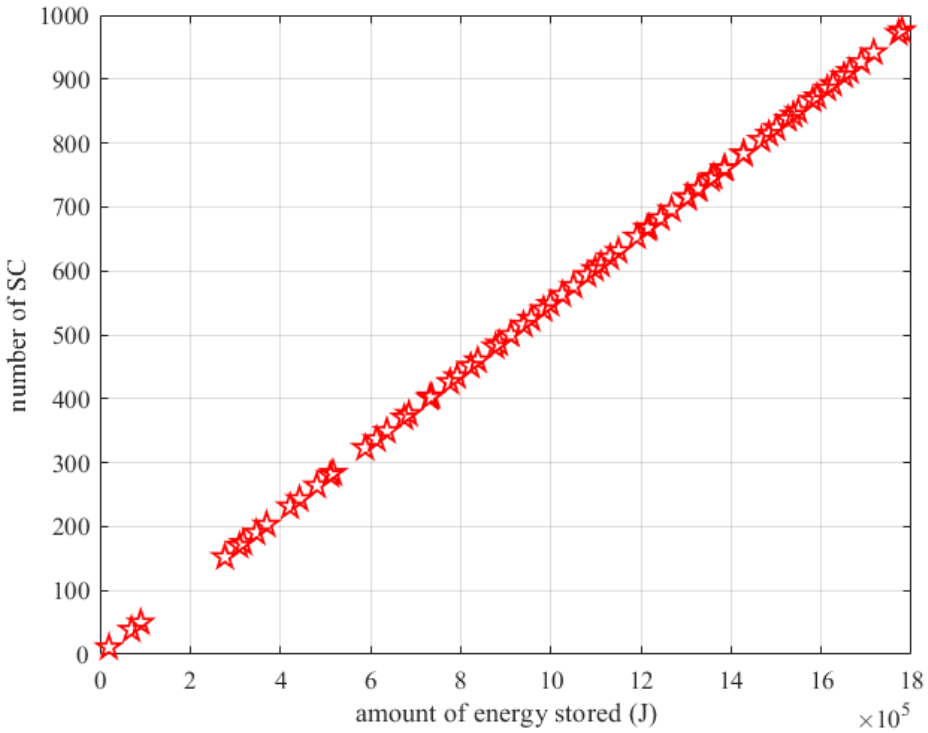

Figure 3-1: Pareto front of the multi optimization model.

A point on the pareto front that corresponds to $n_s = 100$ and $n_p = 4$ is picked because an even number of n_p is required for one of the proposed control strategies, which is discussed later in the report.

Table 3-2: Optimal supercapacitor bank specifications.

Specifications per SC bank	**Value**
Number of series SC, n_s	100
Number of parallel SC, n_p	4
Total Voltage of SC bank (V)	270
Total capacitance of SC bank (F)	20

3.3. Battery Bank

The size of the battery bank used to model the Simulink circuit in the simulations is presented in Table 3-3.

Table 3-3: Battery bank specifications.

Specifications per Battery bank	Value
Rated Voltage (V)	330
Rated Capacity (Ah)	56.3
Response Time (s)	20

3.4. Proposed Strategy

One of the main objectives of this thesis is to develop a novel method to manage the energy flow in the hybrid battery-SC energy storage system. Section 2.4, in this thesis, outlined the different energy flow control methods reported in the literature. In this work, the method approached to solve the problem is RB control method and is developed based on understanding and intuition. While designing the strategy proposed in this work, there are two sought goals: efficiency and practicality. Efficiency of the algorithm refers to the optimal utilization of stored energy while taking into consideration the low energy density of the SC and low power density of the Li-ion battery. Therefore, the proposed energy management algorithm must be careful with the duration where the SC is active to avoid fast depletion and supply the required high current demand from SC to prevent battery aging. Achieving this objective will result in an efficient system. The second objective is to achieve practicality. To have a practical system that can be realized, complexity must be avoided. Building a relatively simple logic that does not require complex hardware achieves practicality for experimental implementation.

Two different energy flow control strategies have been developed in this thesis, one for urban and highway driving cycles and the other for low-speed zones such as residential areas or university campuses.

3.4.1 Control method for urban and highway driving cycles

In the case of medium/high speed driving cycles that usually occur in urban roadways and highway, the motor current demand is usually higher compared to that in a low-speed zone. At the initial stages of this work, a power-smoothing method was proposed [7]. In this approach, the processor detects a sudden increase in current, which activates the SC and then the power output decreases while being compensated by the battery;

therefore, a sudden high current demand from the battery is prevented. However, this algorithm is impractical for the following reasons: the duration of compensation process might be lengthy depending on how fast the closed loop system reacts, which might deplete the SC. Second reason is the unpredictable power demand and fluctuations, which make it difficult for the processor to operate both DC converters accordingly.

The aforementioned method detects the voltage needed across the DC motor. Due to the impracticality explained, this needs to be tweaked and adjusted. Firstly, instead of tracking voltage, it is wiser to track current and operate SC accordingly, since the current demand cannot be easily estimated from voltage values. This is because, the voltage across the DC machine is proportional to its speed, while the current demand is proportional to the torque required to move the car. Therefore, dealing with voltage leaves the current unknown and the energy stored is not used wisely. Instead, the proposed energy management strategy in this thesis tracks the current. This is detailed in Figure 3-2.

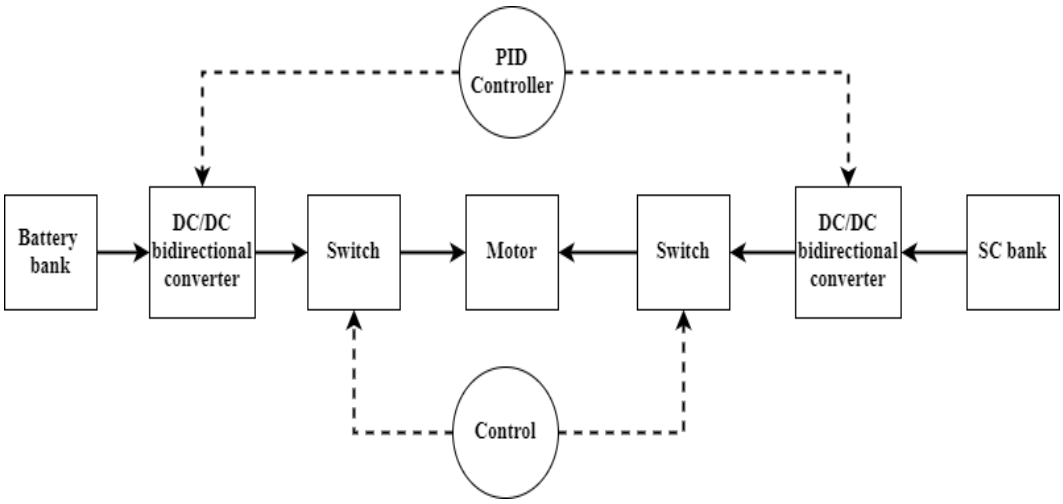

Figure 3-2: Block diagram of circuit connection for urban and highway driving cycles.

The updated energy flow control system, shown in Figure 3-2, no longer performs power smoothing. Instead, it involves a constant feeding of current values into the processor. The frequency with which the data is being logged depends on the processing power. The processor logs one value and stores it, then compares the present current value with the previously stored current value and detects the rate of increase. Operating at C-rate of 2C or more, is essentially harmful to the EV battery and degrades it quickly

[60]. Therefore, if the system detects a rise in current equivalent to 2C, the SC operates and the battery stops supplying energy to the motor. The processor detects this sudden increase corresponding to 2C which reflects high increase in current and the operation is handled by the supercapacitor. Since the logging frequency is high, and the detection occurs very fast, the battery will not have enough time to react to this sudden change and will be protected. Upon switching back to battery, the current and voltage of the circuit will not be altered, because there is an inductor with stored charge acting as a current source and the capacitor across the motor acts as voltage source and the transition will be smooth. By implementing this strategy properly, an efficient and non-complex system is achieved.

Furthermore, taking into consideration the low energy density of SC, the detection circuit can also be used for different purpose. If the circuit detects a negative rate, which corresponds to braking, this negative energy can be used to charge the SC with a process known as regenerative braking. Lastly, a current limit is set for the SC to prevent it from fast depletion, so that if the current goes beyond that threshold, only the battery will be operating. By doing so, the battery SoC is partially restored and the high power density of the SC is utilized by allowing it to respond quickly in cases of sudden current increase.

The proposed strategy will be built using Simulink blocks and implemented on the system to run a simulation on a real driving cycle to track the performance and aging of HESS. Additionally, we aim to observe recharging of the SC bank by allowing the DC/DC converter topology to enable regenerative braking, which boosts the efficiency of the system. This will be further elaborated in the next chapter.

A flowchart to represent the workflow and highlight the process is designed to further clarify the strategy implemented in the HESS is shown in Figure 3-3.

3.4.2 Control method for low-speed zones

In low-speed zones, the driving patterns are expected to differ from those in the medium/high speed driving cycles explained previously. A recurring pattern of frequent stopping and acceleration is expected, and the maximum speed is not very high. From this pattern, useful observations can be deduced to make conclusions about important key takeaways in the current flow within the system.

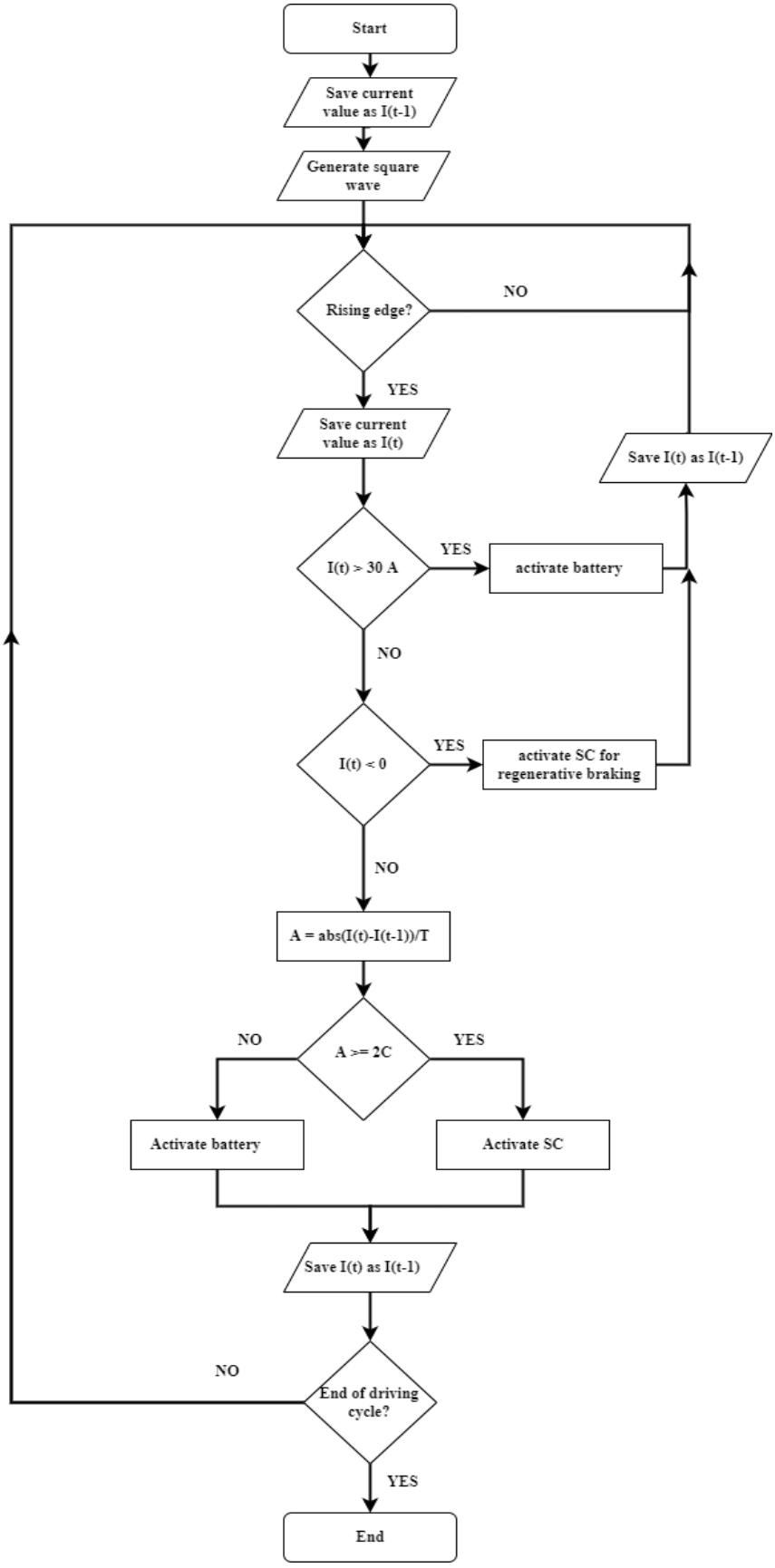

Figure 3-3: Flowchart of the proposed strategy in urban roadways and highway.

Frequent stopping and acceleration will result in high torque to gain inertia, which increases current. This is a very basic concept in motors that starting current is high. Second, the low speed means low current requirement by the motor. Therefore, using power electronics, the circuit can be adjusted on the fly to adapt to these new conditions. The proposed control approach splits the SC bank into two even 10 F SC banks. These 2 SC banks will handle all the energy requirements of the motor. The purpose of the battery in this circuit is only to recharge the depleted SC bank to reoperate in case the other bank is out of charge. The block diagram of the proposed energy flow strategy for low-speed zones is shown in Figure 3-4.

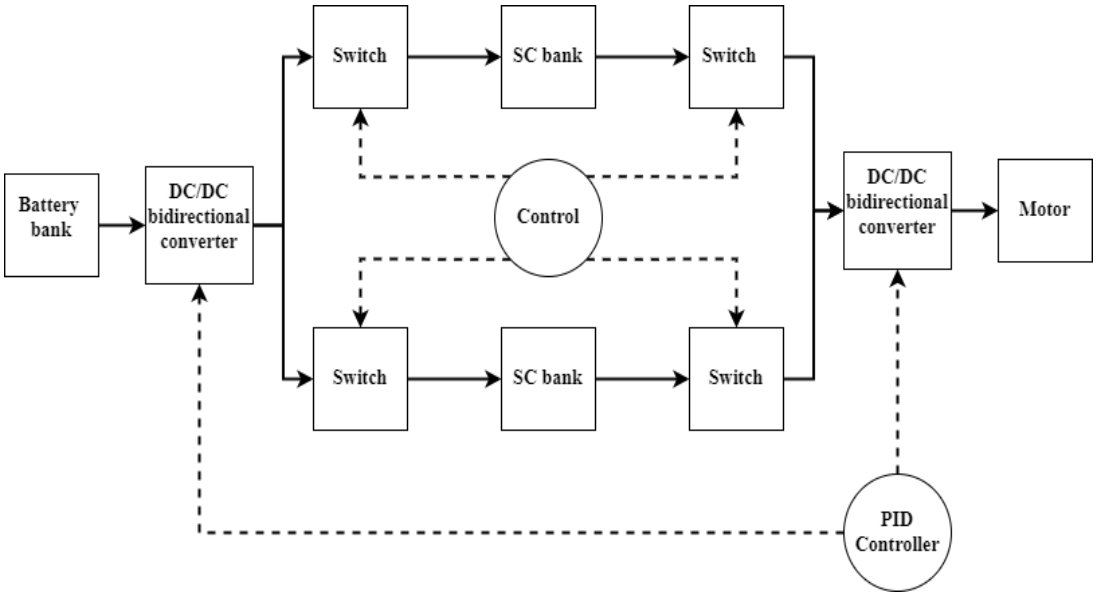

Figure 3-4: Circuit connection block diagram for low-speed driving cycles.

By comparing the topologies in Figure 3-2 and Figure 3-4, the same components are utilized for energy management in both medium/high speed and low speed zones. Simple switching is performed to manage the joint operation of the battery-SC for the different EV driving patterns, i.e., to switch the operation mode of the HESS between the topology in Figure 3-2 and that in Figure 3-4 depending on the driving cycle and is done on the fly. Flowchart of the proposed strategy is illustrated in Figure 3-5.

3.4.3 Reference circuit: Traditional ESS

In order to confirm the advantages of integrating a SC bank, a reference ESS topology is used in which the EV battery is the only source supplying the required energy to the EV motor. This is shown in Figure 3-6.

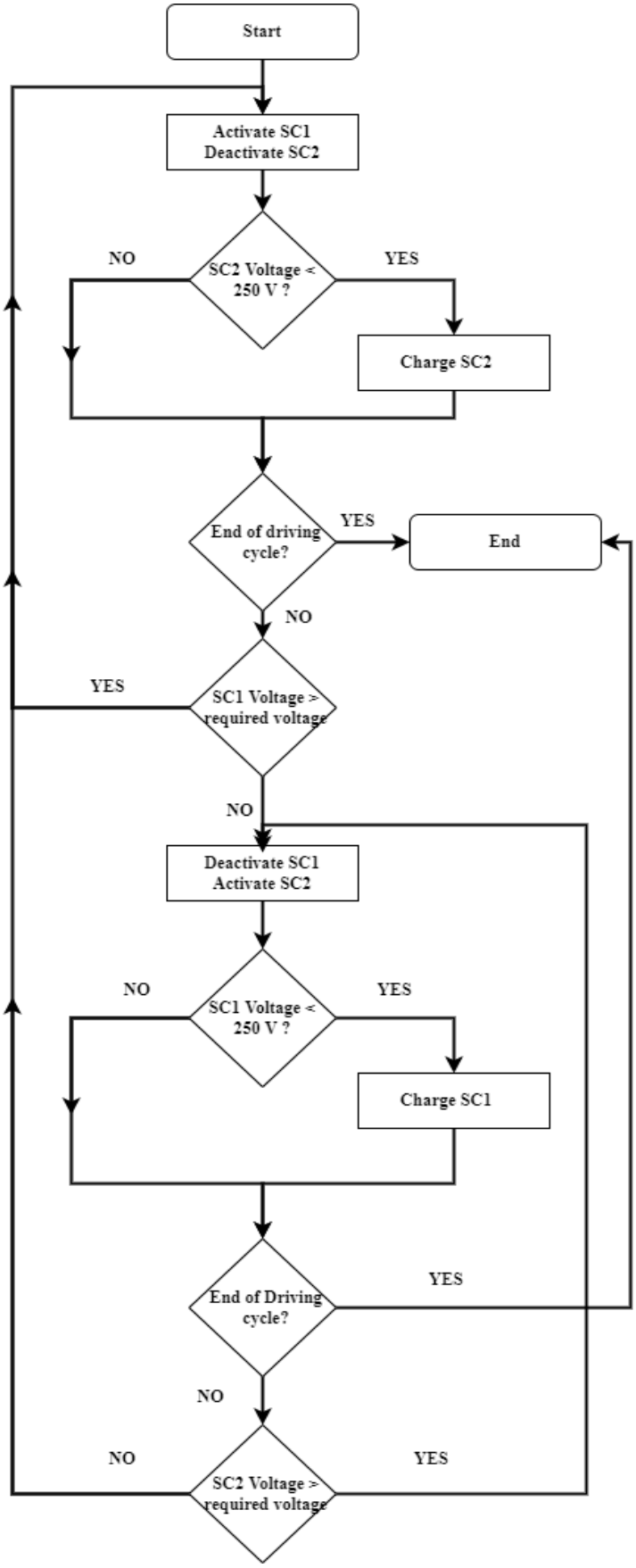

Figure 3-5: Flowchart of the proposed strategy in low-speed zones.

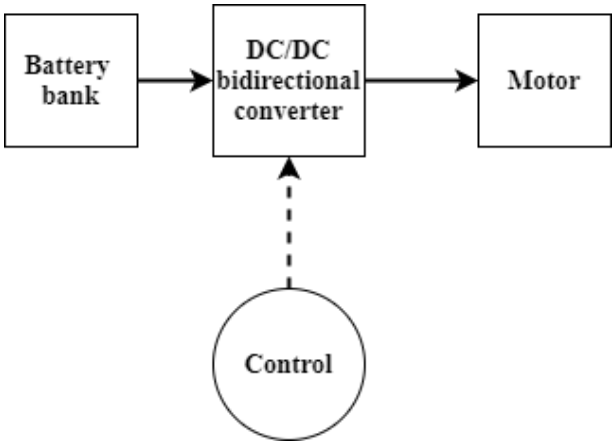

Figure 3-6: Circuit connection block diagram for ESS.

3.5. DC/DC Converter Circuit

Based on the discussion carried out in Section 2.3, the DC/DC converter topology used in circuit design is the DC/DC bidirectional converter for each source, as shown in Figure 3-7. This ensures total isolation of the two sources while allowing the voltage of DC bus to be varied by both sources and the system gains control over the whole circuit.

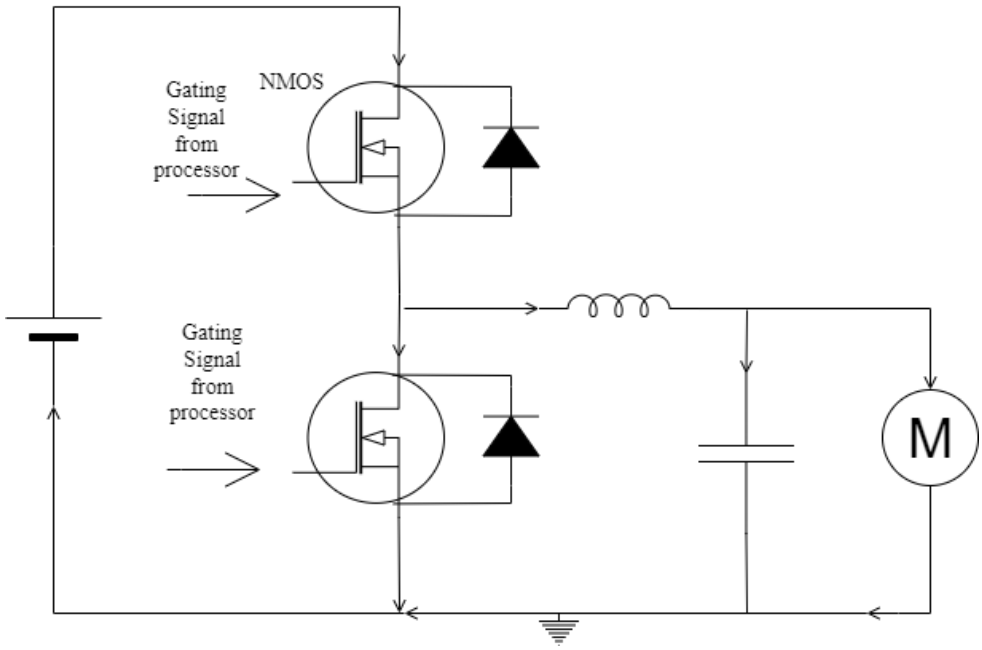

Figure 3-7: Bidirectional DC/DC converter topology.

3.6. Aging Assessment Metrics

As described earlier in the Chapter 2, many papers in the literature present several different methods to evaluate battery aging whether by using empirical approaches or

approximations. Authors in [20] present an elaborate procedure to quantify the loss in capacity by predicting the formation of SEI using different stress parameters.

3.6.1 Thermal stress

Thermal stress occurs because of increase in temperature. The higher the temperature, the higher thermal stress imposed on the battery. To calculate the temperature and to incorporate the cooling effect in the equation, an equation used to model the Li-ion battery in Simulink/MATLAB is adopted to track the internal temperature of the battery. This is a better model than the one previously shown, since cooling effect is involved. First, the temperature-dependent internal resistance of the battery is defined as follows:

$$R(T) = R_{ref} \exp\left(\beta\left(\frac{1}{T} - \frac{1}{T_{ref}}\right)\right). \tag{15}$$

The constant is called Arrhenius constant and it is a negative value because the resistance increases with increase in temperature. The power loss is defined as:

$$P_{loss} = I^2 * R(T). \tag{16}$$

Accordingly, the internal temperature of the battery can be calculated as,

$$T = L^{-1}\left(\frac{T_a + R_{th}P_{loss}}{1 + st_c}\right), \tag{17}$$

where T_a is the ambient temperature, R_{th} is thermal resistance (C/W), and t_c is the thermal time constant.

Knowing the temperature, thermal stress can be quantified as follows:

$$S_T = \exp\left(T_{fact}(T - T_{nom})\frac{T_{nabs}}{T_a}\right), \tag{18}$$

where $T_{fact} = 0.0693$ is the coefficient of temperature in the thermal aging model, T is the actual battery temperature in Celsius, T_{nom} is the reference battery temperature,

T_{nabs} is the reference battery temperature in Kelvin, and T_a is the battery temperature in Kelvin.

3.6.2 Time stress

Time stress is essentially the stress imposed on the battery while it operates. Therefore, as long as the battery is supplying current, time stress is incrementing. It is quantified as:

$$S_t = k_t t, \tag{19}$$

where k_t is a constant and t is the working duration.

3.6.3 SoC stress

SoC stress is the amount of stress handled by the battery when it carries too much charge. Therefore, this stress model indicates a higher degradation rate at high SoC level and a lower rate at lower SoC levels. This is calculated as:

$$S_{SoC} = \exp\left(k_\sigma\left(\sigma - \sigma_{ref}\right)\right). \tag{20}$$

The reference SoC in the calculations carried out in this thesis is the average SoC level of the battery after the driving cycle.

3.6.4 Calendar aging

Using the stress parameters discussed, calendar aging can be quantified as the product of the aforementioned stress factors, as:

$$f_d = S_T S_{SoC} S_t. \tag{21}$$

3.6.5 Loss in capacity

Let α_{SEI} be the portion of the charge capacity irreversibly consumed during the SEI film formation [20]. The normalized capacity is broken down to SEI formation (α_{SEI}) and the portion that fades away proportional to battery life, ($1 - \alpha_{SEI}$), and is modeled as two exponential functions:

$$L = 1 - \alpha_{SEI}\exp(-f_{SEI}) - (1 - \alpha_{SEI})\exp(-f_d). \tag{22}$$

The parameter α_{SEI} appears to be highly dependent on the design of the battery. The authors of [61], [62] and [63] concluded that α_{SEI} depends on the specific surface area of the graphite as well as on the layer formation conditions and that the value of α_{SEI} varies from 3% to 8%.

Since usage and temperature also contribute to SEI formation, f_{SEI} is assumed to be proportional to the calendar aging, f_d, in (21), and the normalized capacity can be rewritten as:

$$L = 1 - \alpha_{SEI} \exp(-\beta f_d) - (1 - \alpha_{SEI}) \exp(-f_d). \tag{23}$$

The capacity is normalized from 0 to 1, with $L = 0$ indicating new battery and $L = 1$ representing the end of the battery life.

Chapter 4. Simulations and Results

In this chapter, the simulation setup for the two proposed energy management strategies is outlined and the simulation results are reported. Performance evaluation of the proposed HESS is performed using the performance assessment metrics detailed in Chapter 3.

4.1. Simulink Setup

The Simulink models for the two proposed HESS control topologies are constructed according to the block diagrams in Figure 3-2 and Figure 3-4, for medium/high speed cycles and low-speed zones, respectively.

4.2. Urban Roadways and Highway

4.2.1 Driving cycle

For simulation concerning urban roadways and highway driving cycle, New York driving cycle [64] in has been considered as it consists of high and low speeds, stopping and accelerations which might refer to traffic lights or traffic jam. The available driving cycle is a 10-minute long cycle, which was not enough to observe significant changes; therefore, the cycle is repeated 6 times to simulate 1 hour driving cycle which is more realistic. Additionally, the voltage level of the cycle was manipulated to reflect higher speeds to put the energy storage system into more stressful conditions and observe how they operate. The resulting driving cycle is shown in Figure 4-1.

The edited driving cycle is fed into the system shown in Figure 3-2 as a reference signal. This makes the Simulink circuit a realistic one. The reference signal is fed into control closed loop and the PID controller outputs a PWM signal with specific duty cycle to the MOSFETS the of DC/DC converter to generate the required amount of voltage across the motor and the output voltage level must be close to the reference signal. Switching of the power sources is controlled by the control strategy that is described previously and is implemented on Simulink using blocks and lines of the code to observe the operation of the system and eventually witness the enhancements and improvements the auxiliary source adds to the system.

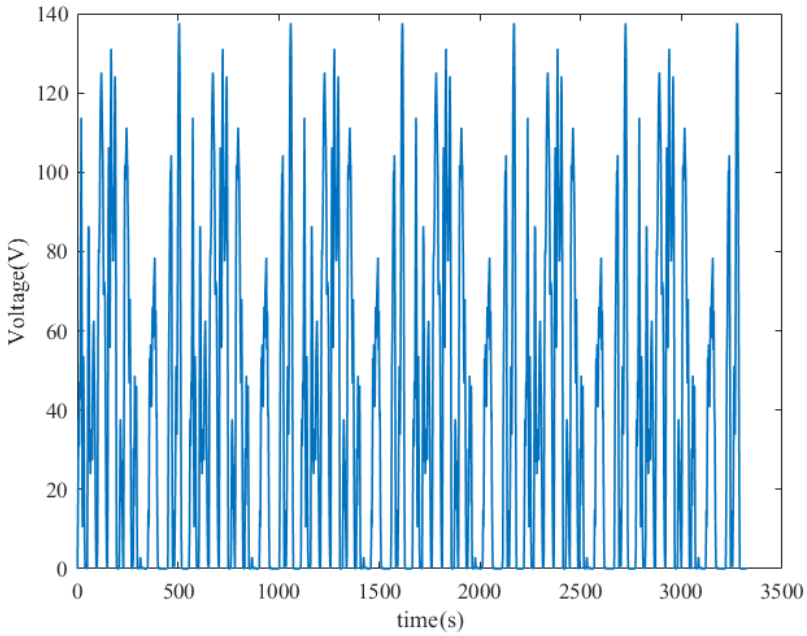

Figure 4-1: Driving cycle used to simulate the HESS control strategy developed for urban roadways and highways.

4.2.2 Simulation results

First, it is crucial to compare the reference signal with the PID output signal to observe whether they match or not. This verifies the performance of the closed loop used to track the required output voltage level. This is shown in Figure 4-2.

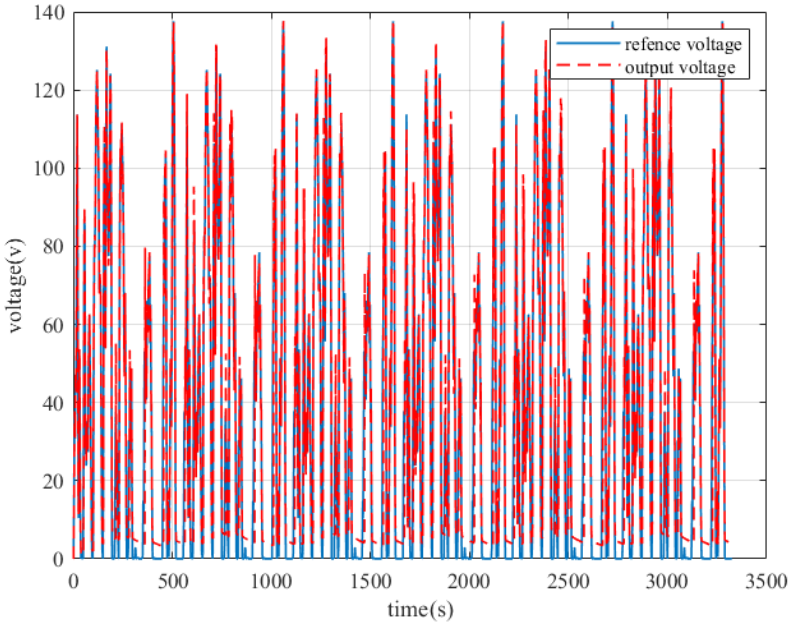

Figure 4-2: PID output signal and voltage reference signal.

As can be seen from Figure 4-2, the output voltage and reference voltage are almost a perfect match which shows that the designed closed loop is functioning properly. To assess the difference between the output voltage and reference voltage, a plot showing the absolute difference is presented in Figure 4-3.

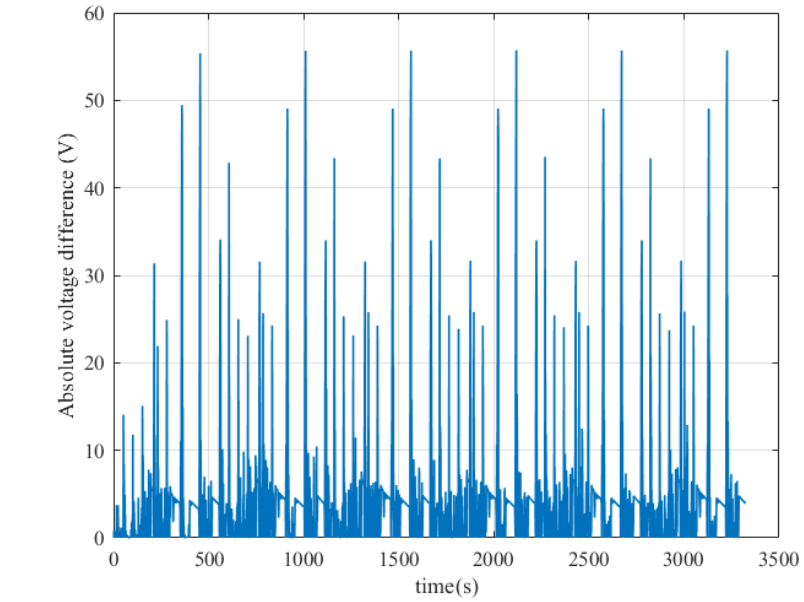

Figure 4-3: Absolute voltage difference between output voltage from PID and reference voltage.

Secondly, the current demand by the motor is shown in Figure 4-4.

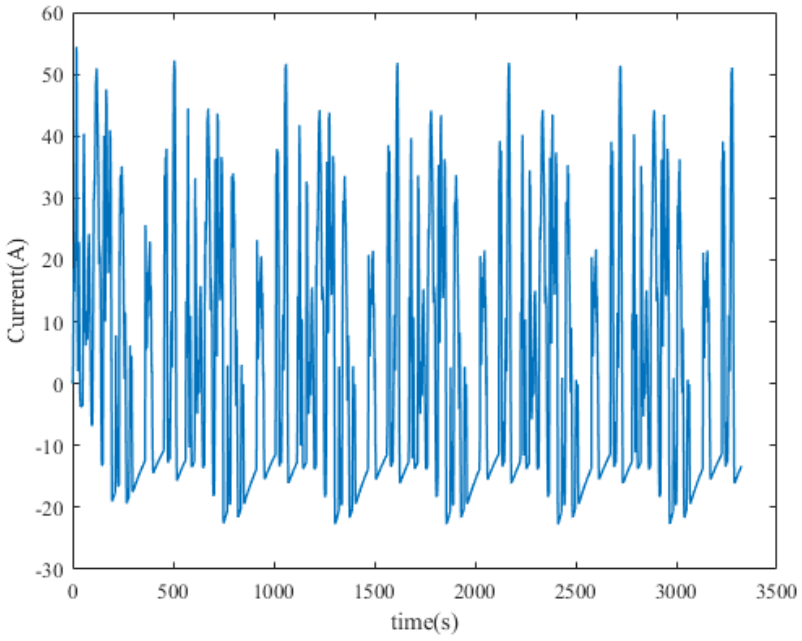

Figure 4-4: Current demand of EV motor throughout the driving cycle.

The current demand of the EV motor is addressed by the SC and the EV battery according to the implemented control method. Figure 4-5 shows the current flow from each source and a small window of time to demonstrate what happens clearly. It can also be noticed that negative current is sourced from SC, which represents the regenerative process that charges the SC bank.

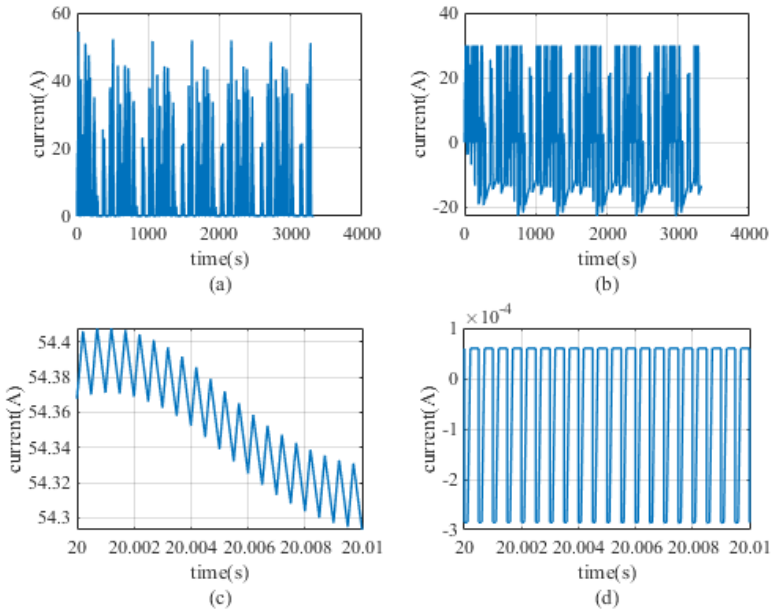

Figure 4-5: Current output to the EV motor from the battery and the SC: a) battery's output current, b) supercapacitor's output current, c) battery's output current in short time interval from 20s to 20.01s, d) supercapacitor's output current in the same time interval.

The SoC of battery and SC are plotted in Figure 4-6.

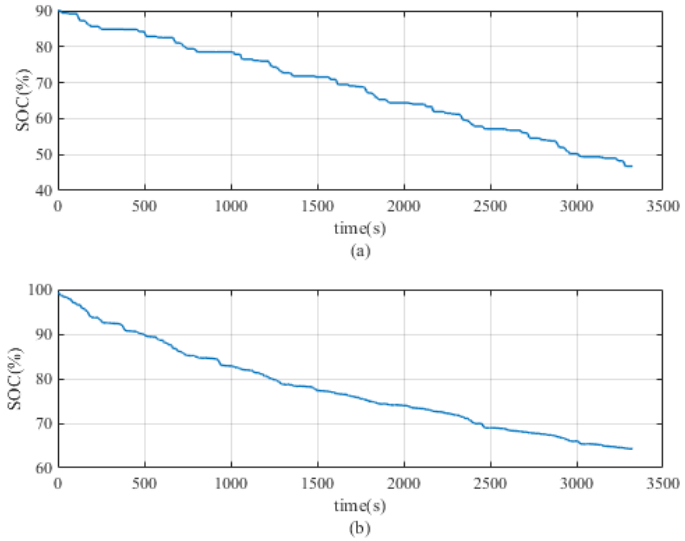

Figure 4-6: SoC of the battery and the SC during the 1-hr driving cycle: a) battery's SoC, b) SC SoC.

The traditional battery-only ESS in Figure 3-6 is then simulated using the same driving cycle and the SoC of battery bank is plotted as shown in Figure 4-7.

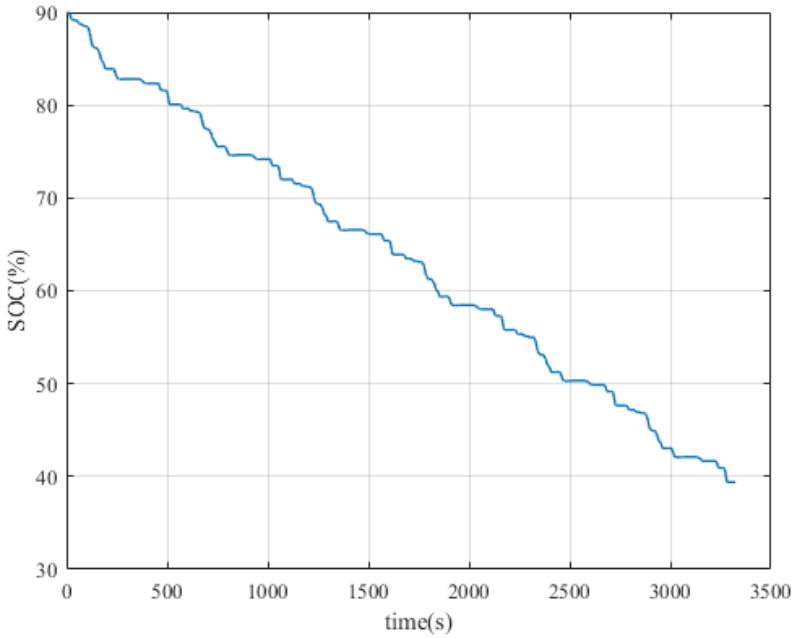

Figure 4-7: Battery's SOC level in traditional battery-only ESS.

From Figure 4-6 and Figure 4-7, it can be deduced that 10% of SOC is saved in HESS. The different stress factors imposed on the battery with and without SC bank are then studied as follows.

4.2.3 Performance evaluation

4.2.3.1 Thermal stress

To quantify thermal stress, temperature rise is evaluated first using (17). This is plotted in Figure 4-8.

It is observable that there is a dramatic decrease in temperature rise in HESS compared to ESS. The temperature difference is reflected in thermal stress calculation. Thermal stress on the battery bank is shown in Figure 4-9.

As observed in Figure 4-9, a noticeable reduction in the overall thermal stress occurs when SC bank is employed. The observed fluctuations in Figure 4-8 and Figure 4-9 are due to the fluctuations in the motor current required for the simulated driving cycles.

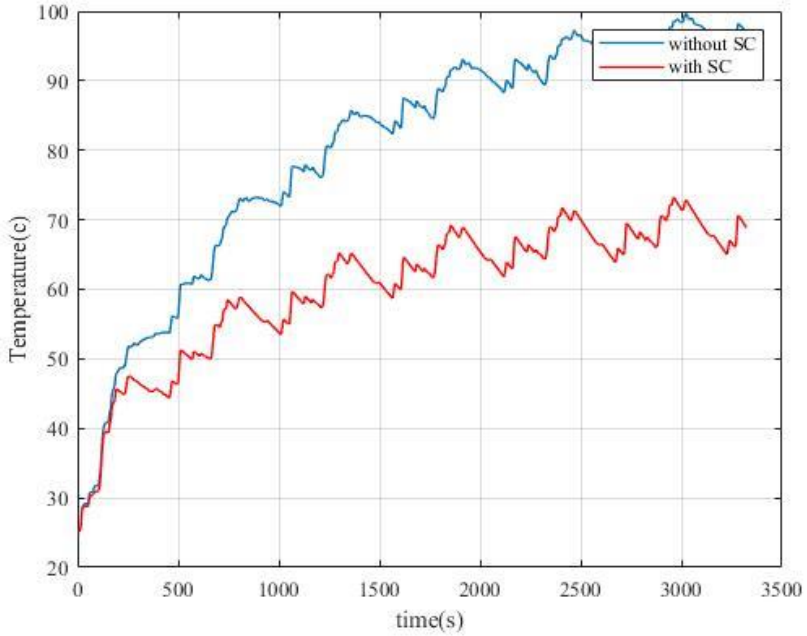

Figure 4-8: Comparison of battery's temperature in ESS and HESS.

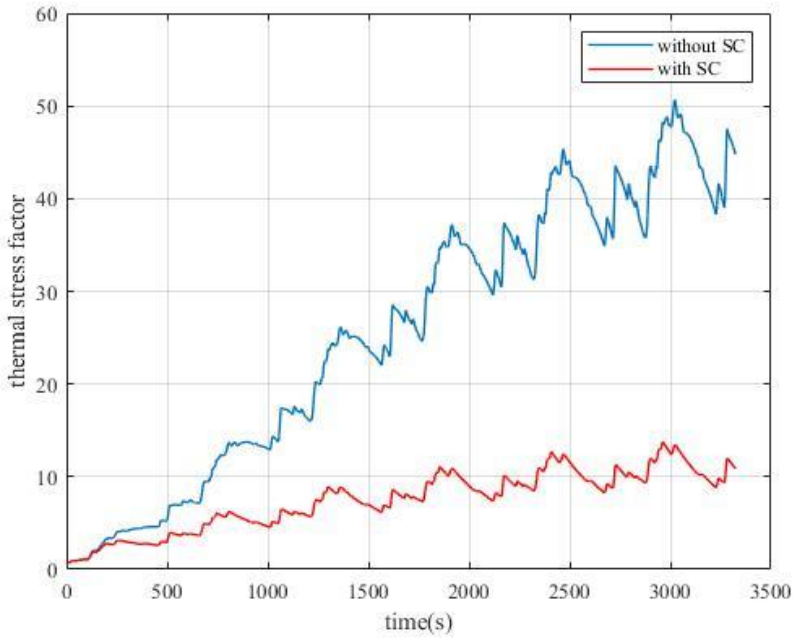

Figure 4-9: Comparison of battery's thermal stress in ESS and HESS.

4.2.3.2 Time stress

Expectedly, the time stress on the battery with SC will be less compared to battery without SC, since battery stops operating when SC is active, hence the total time of operation is less. This is verified in Figure 4-10.

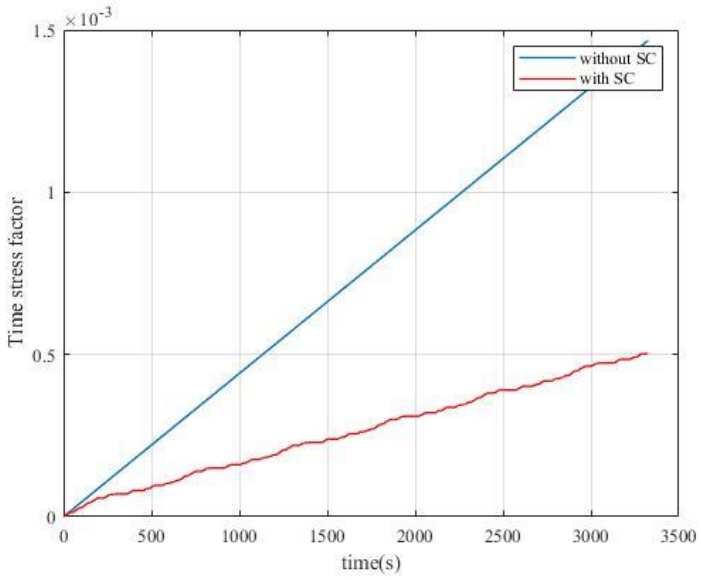

Figure 4-10: Comparison of battery's time stress in ESS and HESS.

As expected, the time stress on the battery in HESS is significantly lower than that in the ESS, since battery is not operating throughout the whole cycle.

4.2.3.3 SoC stress

SOC stress varies according to the average and current SoC of the battery. The impact of this stress factor gives an advantage to the traditional ESS without SC, as shown in Figure 4-11. However, using SC stores more battery charge during operation and the impact of SoC stress is not significant.

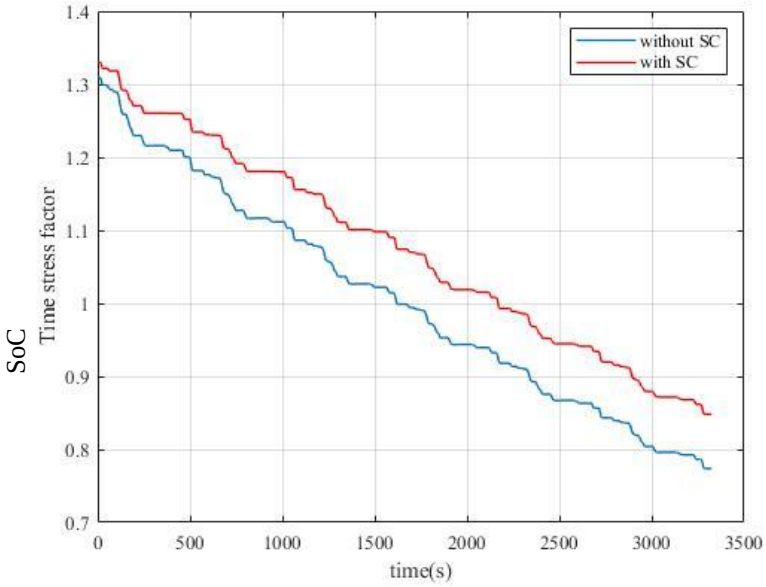

Figure 4-11: Comparison of battery's SOC stress in traditional ESS and HESS.

4.2.3.4 Calendar aging and loss in capacity

The corresponding calendar aging as a result of the resulting stress factors and the cumulative loss in capacity is described in Figure 4-12 and Figure 4-13, respectively.

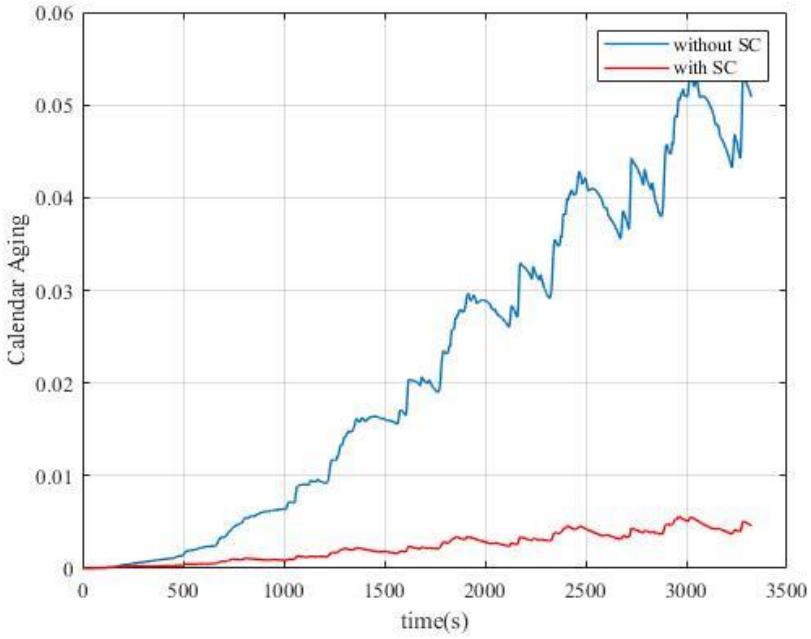

Figure 4-12: Battery's calendar aging in traditional ESS and HESS.

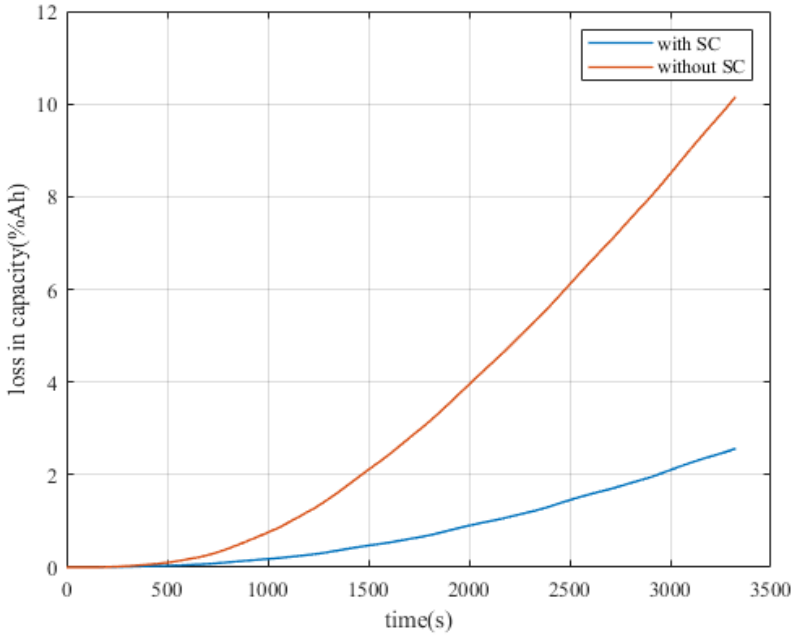

Figure 4-13: Battery's percentage loss of capacity in traditional ESS and HESS.

Based on the presented result, the loss incurred using SC is 2% of the actual capacity compared to 10% of battery's capacity in ESS, which indicates 5 times reduced aging. Therefore, the battery's lifetime is approximately extended by 5 times after integrating SC, when acknowledging urban and highway driving patterns. In addition to the increase of lifetime, it can also be noticed that there is almost 20% more SOC stored in the battery in HESS which indicates longer driving range. Moreover, it is observed that the SC did not deplete by the end of the driving cycle. Nevertheless, it should be noted that the constants in stress equations are taken from [20] and these values might be different for the battery model in Simulink.

4.3. Low Speed Zones

4.3.1 Driving cycle

For this scenario, a widely used driving cycle called US06DC is used [64]. The original cycle duration of 10 minutes is used since a typical driving cycle around a campus, or a residential area is expected to span around 10 minutes. The driving cycle used is illustrated in Figure 4-14.

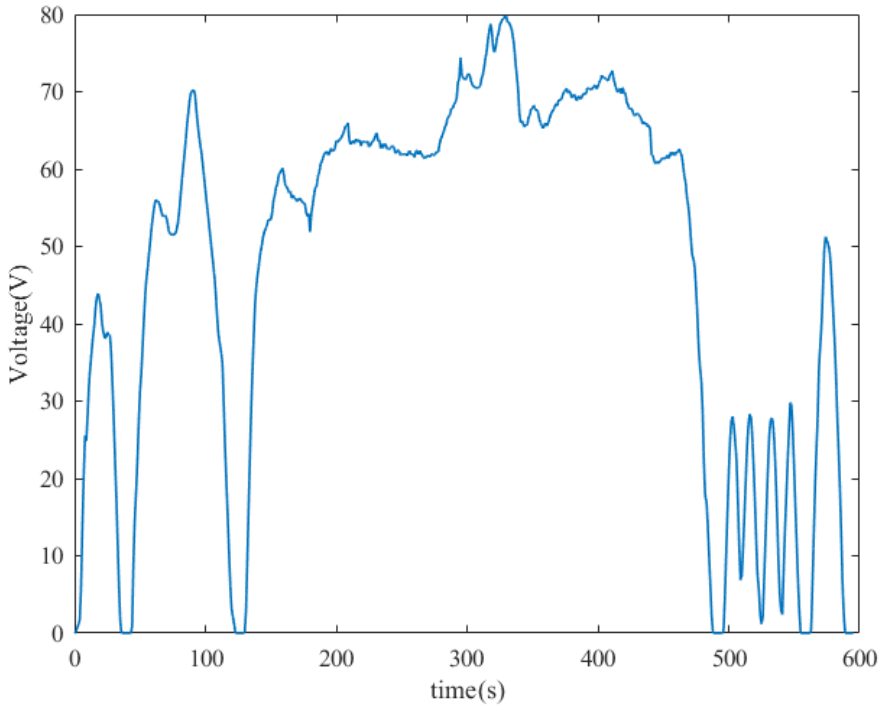

Figure 4-14: Driving cycle used to simulate control method developed for low-speed zones.

4.3.2 Simulation results

Using the driving cycle shown in Figure 4-14 and the circuit diagram in Figure 3-4, low-speed zone simulations are carried out. First, the closed loop is verified by checking how the output signal is following the reference signal, as shown in Figure 4-15.

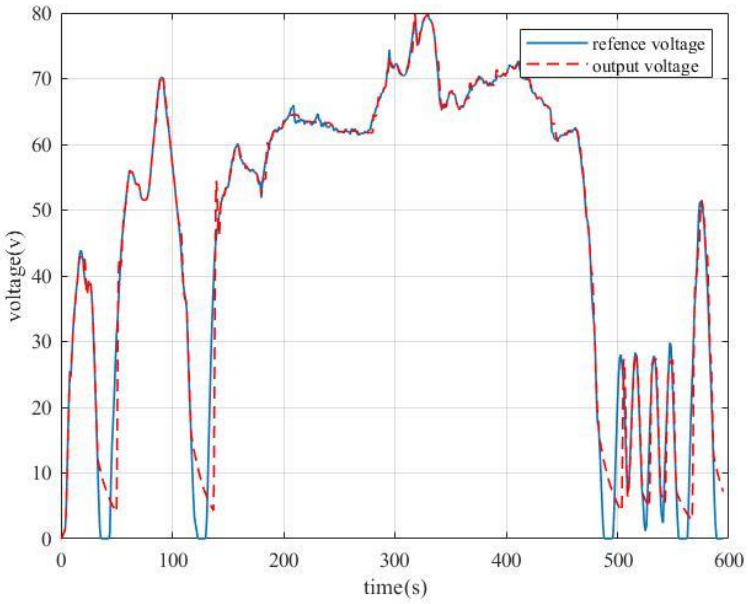

Figure 4-15: PID output signal and voltage reference signal.

Similarly, a plot showing the absolute difference of the output and reference voltages is created to observe the performance of PID controller and is shown in Figure 4-16.

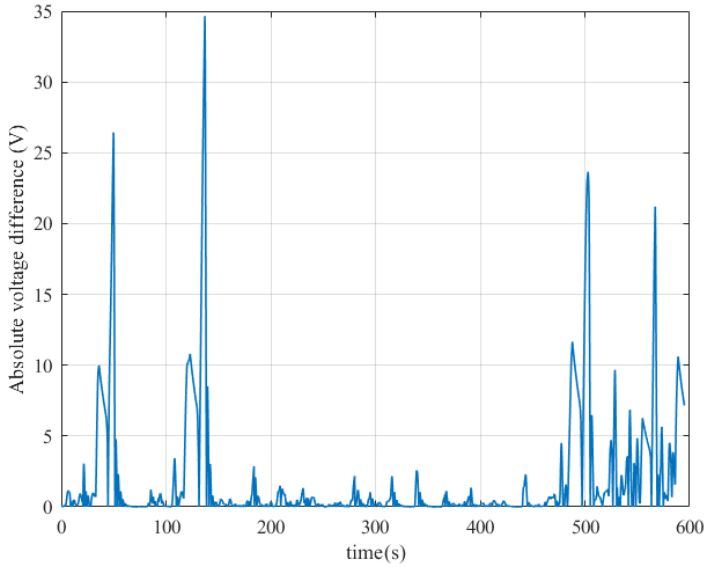

Figure 4-16: Absolute voltage difference between reference voltage and PID output voltage.

As shown in Figure 4-15 and Figure 4-16, the PID follows the reference signal as desired. Since the EV battery in this scenario is only used to charge the SC banks, the voltage levels of the two SC banks is then plotted as shown in Figure 4-17.

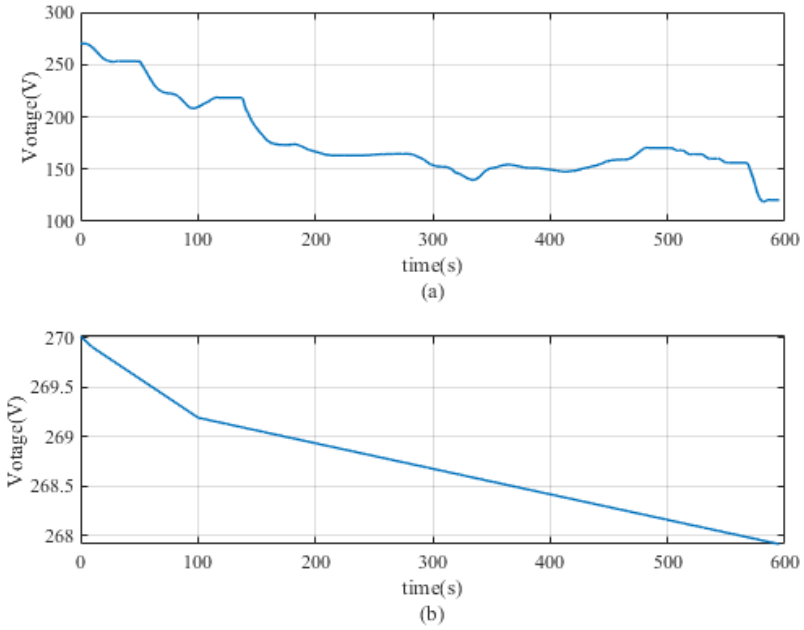

Figure 4-17: Voltage levels of the two SC banks during the 10-min low-speed driving cycle: a) voltage of 1st SC bank, b) voltage of 2nd SC bank.

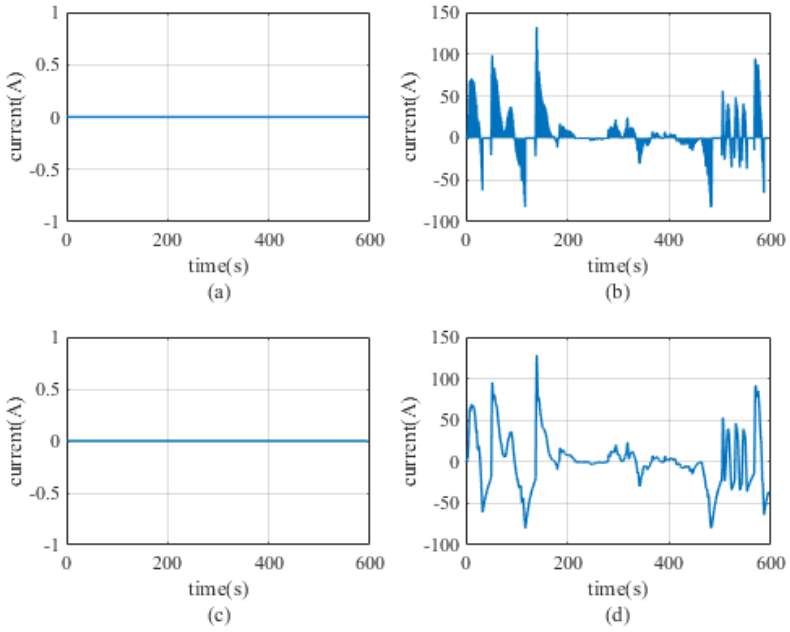

Figure 4-18: Current levels of the different system components: a) battery's output current, b) first SC bank output current, c) second SC bank output current, and d) motor current demand.

As observed in Figure 4-17, only one SC bank is operated for the 10-minute driving cycle, while the second SC is only slightly depleted due to leakage. This means that only one SC bank was able to handle the entire 10-min driving cycle. A summary of output current is shown in Figure 4-18.

As explained previously, a very high starting current is observed followed by a deep dip in current representing regenerative braking, then a very low current almost 0 during the part where voltage is steady. This is confirmed by the patterns shown in Figure 4-18.

It is desired to see how the system reacts in more strenuous and aggressive conditions, and more importantly, to verify whether the SC without the help of battery will be able to provide motor with enough power throughout the cycle. Therefore, the driving cycle was manipulated a little to increase the current demand. The system is compared with the traditional ESS without SC bank. Similar to previous analysis, the different stress factors are compared for both HESS and ESS.

The current flow dataset with the new driving is shown in Figure 4-19, and the corresponding voltage levels of the battery and SC are shown in Figure 4-20.

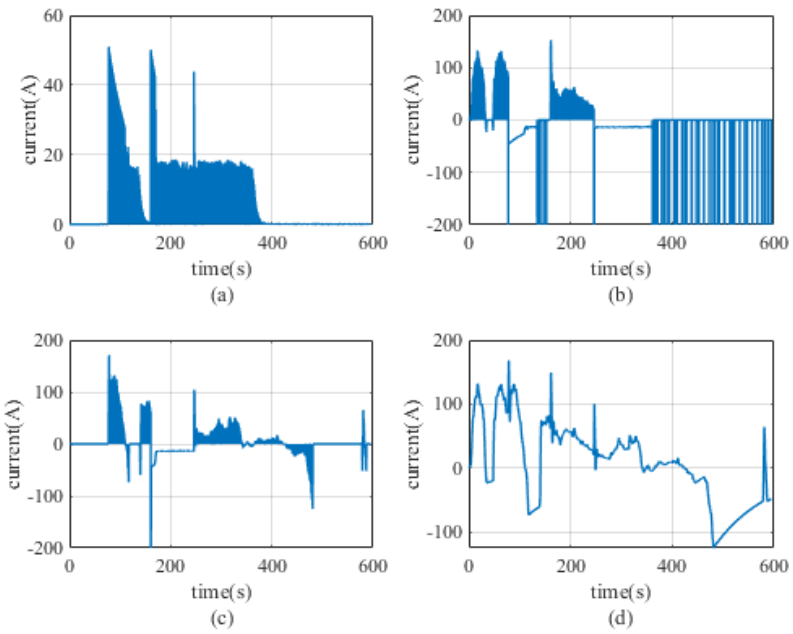

Figure 4-19: Current levels of the different system components for the modified low-speed driving cycle: a) battery's output current, b) first SC bank output current, c) second SC bank output current, and d) motor's current demand.

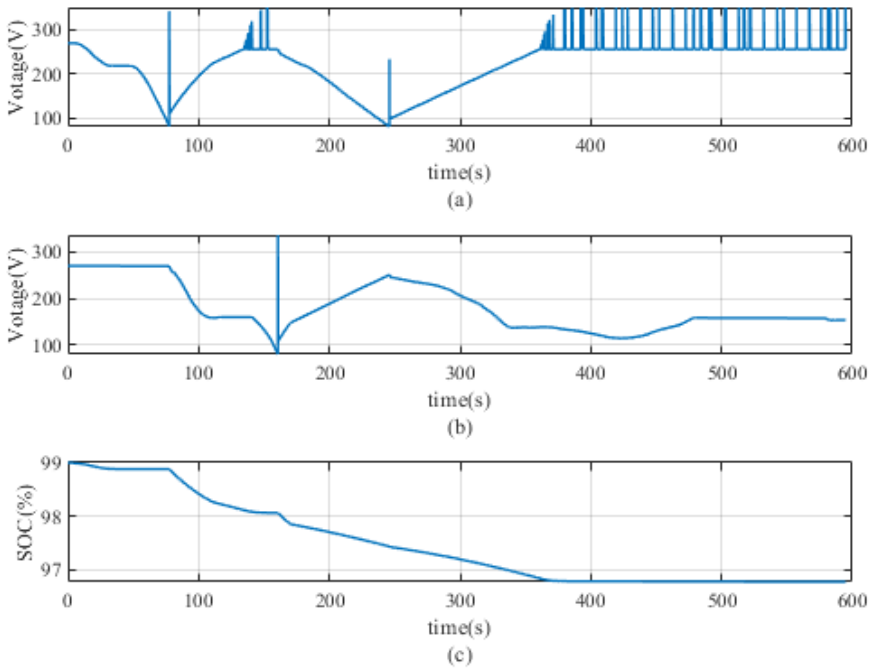

Figure 4-20: Voltage levels and SoC for the modified low-speed driving cycle: a) voltage level of first SC bank, b) voltage level of second SC bank, and c) battery's SOC level.

The traditional battery-only ESS in Figure 3-6 is then simulated using the same driving cycle and the SoC of battery bank is plotted as shown in Figure 4-21. This is compared to the SoC of the battery in the HESS in Figure 4-20(c).

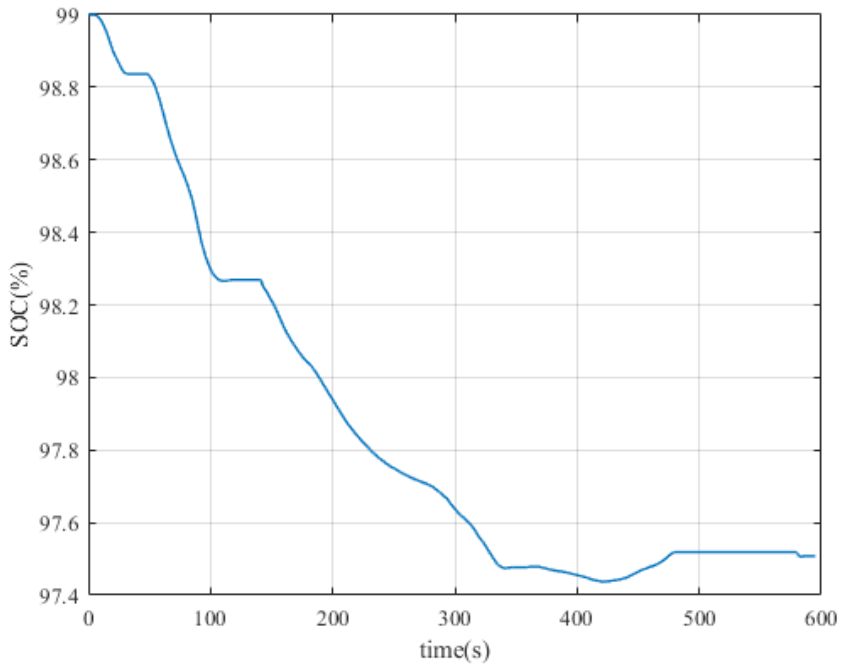

Figure 4-21: Battery SoC level in the traditional battery-only ESS.

4.3.3 Performance evaluation

4.3.3.1 Thermal stress

First, the rise in internal temperature is approximated using (17), as shown in Figure 4-22.

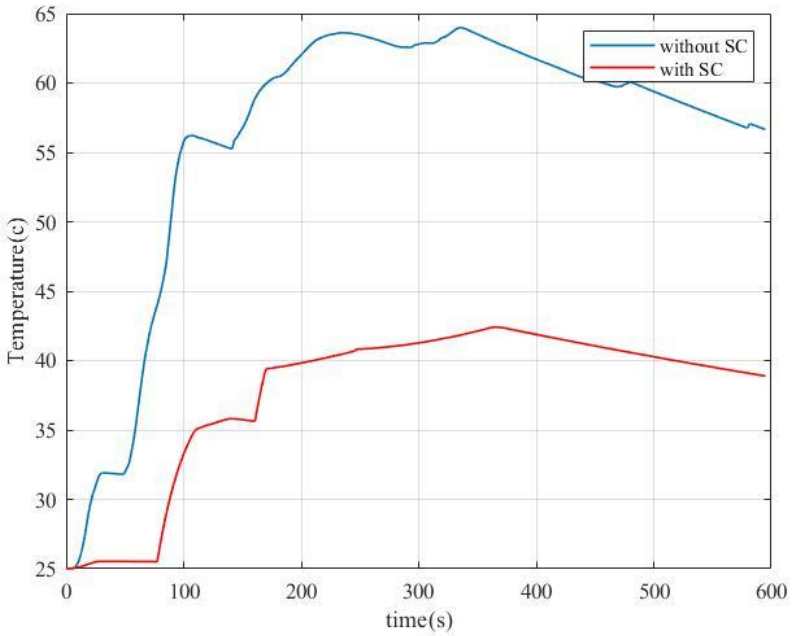

Figure 4-22: Battery's temperature variation in traditional ESS vs HESS.

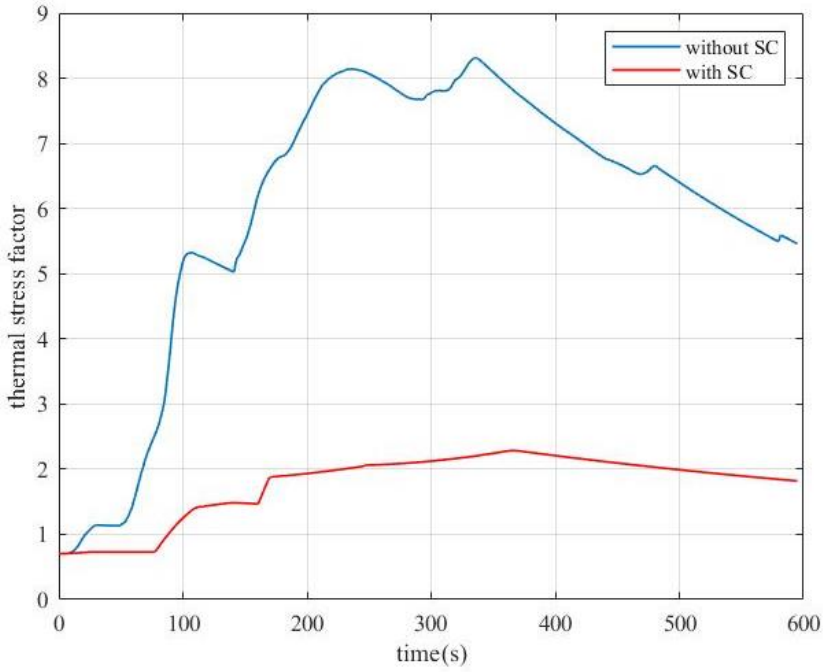

Figure 4-23: Thermal stress variations in ESS and HESS.

Similar to the performance in the medium/high-speed driving cycle, the temperature rise in ESS is higher compared to the HESS, and this is due to the high current output from the battery in ESS. Thermal stress due to rise in temperature is shown in Figure 4-23.

The pattern represented in Figure 4-22 is followed in Figure 4-23, which confirms the higher thermal stress in the traditional ESS compared to HESS.

4.3.3.2 Time stress

Time stress for both cases is shown in Figure 4-24. Similar to the performance in the medium/high speed cycles, the battery in the HESS is not continuously working and operates only when necessary, whereas current flows in and out of battery non-stop in ESS. This translates into a higher time stress in the traditional ESS.

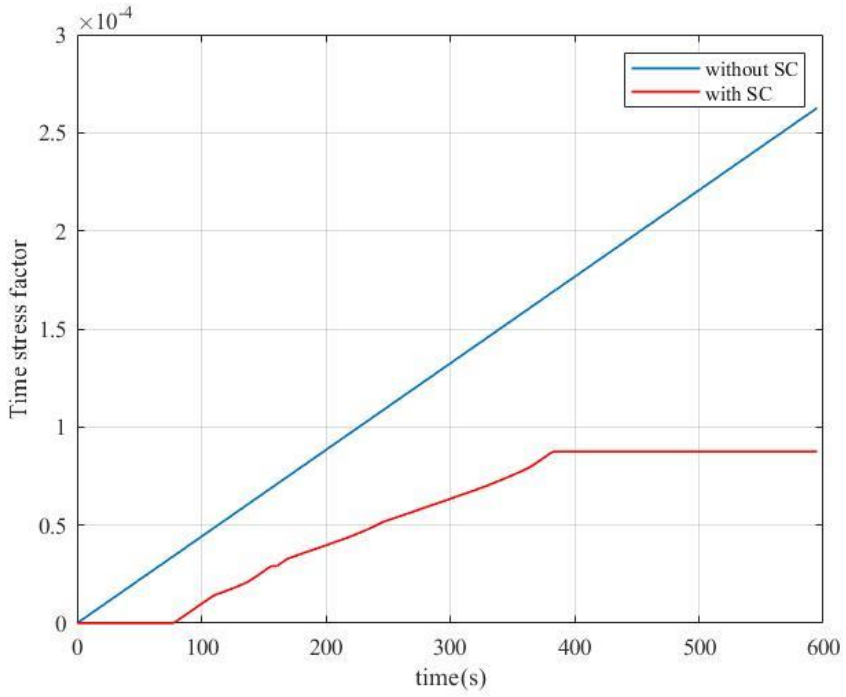

Figure 4-24: Time stress variations in ESS and HESS.

4.3.3.3 SoC stress

The SoC stress is described in Figure 4-25. It can be noticed that the loss in SoC is almost the same for both scenarios, which could be due to the lower capacity of battery in HESS to compensate for the size of SC. Therefore, the SoC drop happens faster in HESS as the battery is smaller.

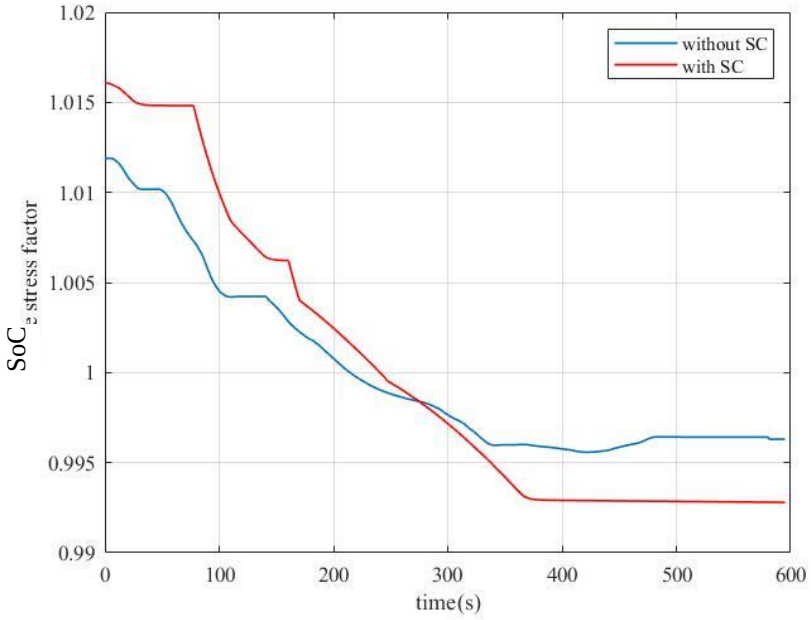

Figure 4-25: SOC stress imposed on the battery in ESS and HESS.

4.3.3.4 Calendar aging and loss in capacity

Acknowledging the rise in temperature due to high current demand as shown in Figure 4-22, the stress imposed on the battery in the traditional ESS is more, which can be observed in Figure 4-26 and Figure 4-27 describing the calendar aging and the cumulative loss in capacity, respectively.

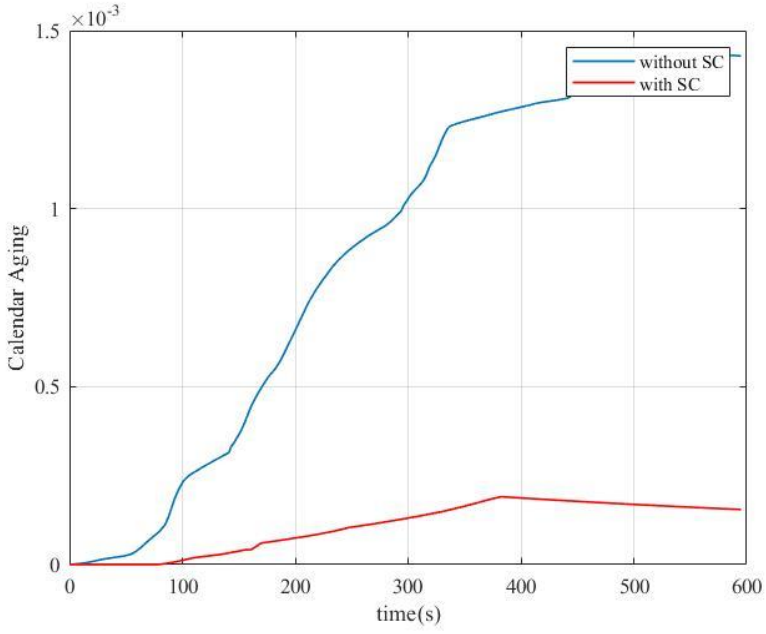

Figure 4-26: Resulting calendar aging in ESS and HESS.

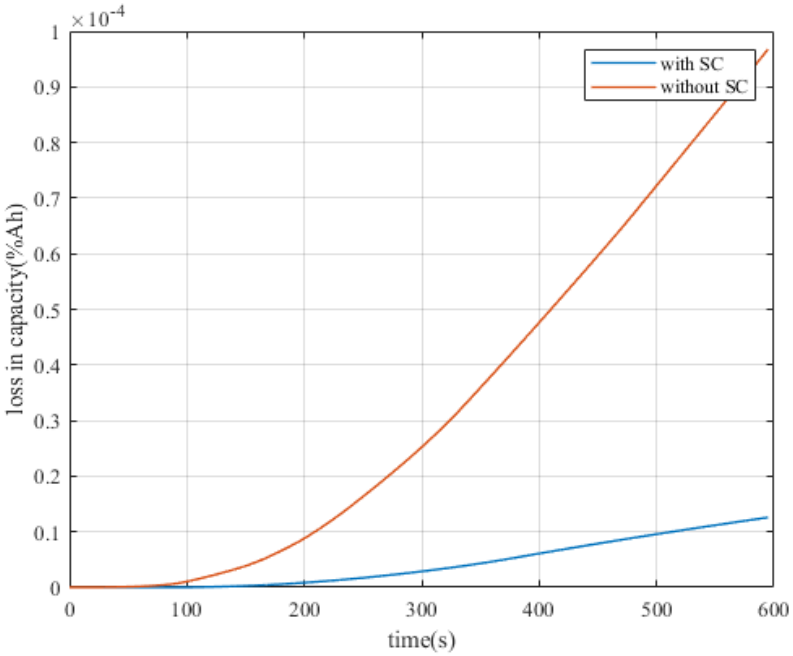

Figure 4-27: Battery's percentage capacity loss in ESS and HESS.

It can be noticed here as well that an improvement of slightly more than 5% occurs in this system. Therefore, a constant pattern can be observed.

4.4. Key Takeaways

It can be clearly illustrated from the figures in this section that a noticeable significant improvement and enhancement occurs in the HESS using the proposed energy management strategy. An observable reduction in battery's internal temperature which reflects in decrease in the corresponding thermal stress. Additionally, time stress is reduced, since battery does not operate the whole driving cycle during the operation of SC bank. SoC stress in HESS is more, but this is compensated by longer driving range as the SoC of battery in HESS is higher than ESS in urban roadways and highway scenario. Lastly, according to equation (23) modeling the loss in capacity, a noticeable improvement showing decrease in the loss of capacity in HESS compared to ESS during the same driving cycle.

Chapter 5. Experimental Verification

5.1. Experimental Setup

To verify the operation and performance of the proposed energy management strategies for the HESS, an experimental prototype is implemented.

The circuit used for the experimental setup aims to mimic the circuit and control strategy used in the Simulink model but on smaller scale. This is shown in Figure 5-1.

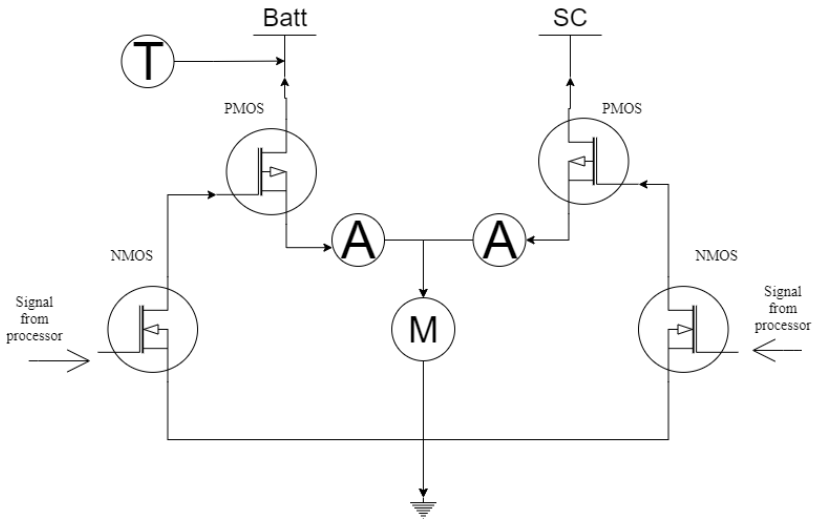

Figure 5-1: Schematic diagram of the implemented prototype.

The circuit in Figure 5-1 is implemented using the components listed in Table 5-1, as shown in Figure 5-2. A similar circuit with the same sensor is used without SC bank for comparison, which was also subjected to the same driving cycle conditions.

Table 5-1: List of components used in the circuit.

Component	Manufacturer	Model Number	Quantity
H-bridge motor driver	STMicroelectronics	L298n	2
Optocoupler IR speed sensor	Aexit	LM393	2
Temperature sensor	Bolsen	LM35	2
Current sensor	Allegro® MicroSystems	ACS712	3
P-type MOSFET	Eaton	RF9640	2
N-type MOSFET	Eaton	IRF540	2
Microcontroller	Arduino	Arduino Mega 2560	1

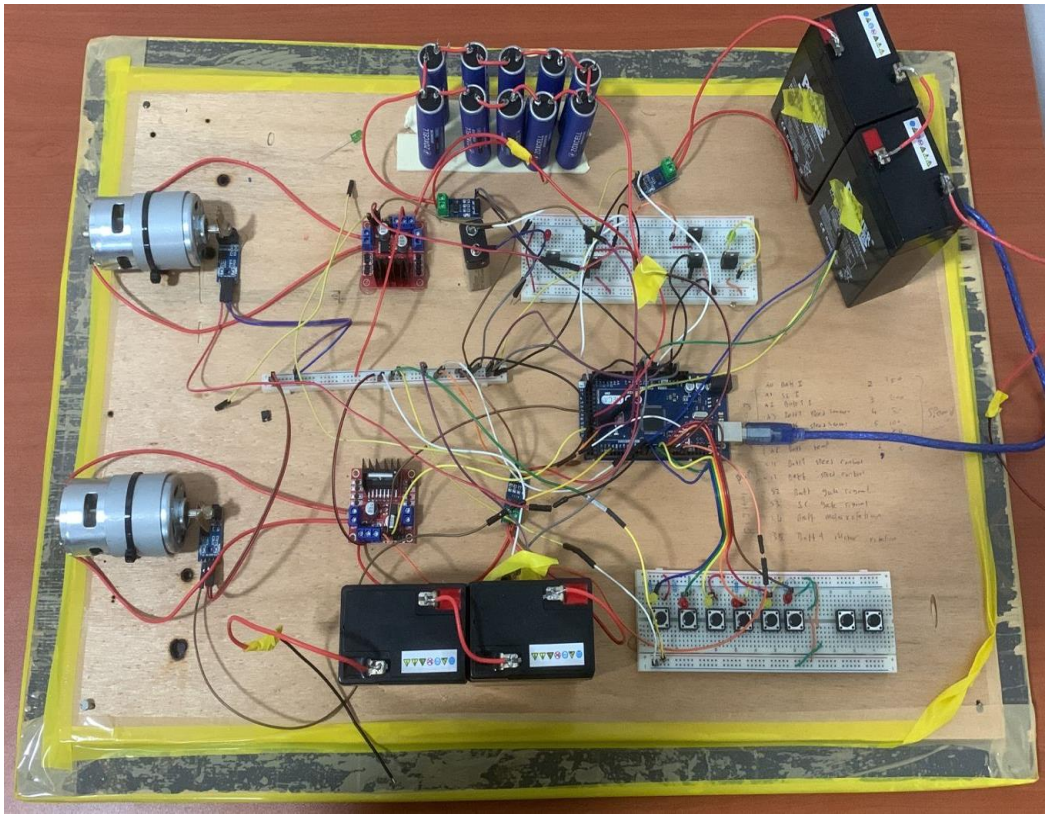

Figure 5-2: Circuit for experimental model.

For the DC/DC converter, an H-bridge L298n model is used. The battery with specs mentioned previously is replaced with 12V 4.5 Ah battery. The SC bank is made of 5 ZOXCELL 3000F 2.7V SC cells in series and 2 in parallel forming a 1200 F, 13.5V SC bank. ACS712 device is a current sensor used to track the current flowing into the motor from each source. LM393 IR optocoupler is used to measure the speed of the motor. A piece of cardboard is attached on the shaft of the motor that cuts the optocoupler connection raising the signal from 0 to 1. The rising of the square signal can be used to measure the speed. Lastly, the driving cycle is created using a speed control unit that consists of multiple buttons, with each button corresponding to a specific value of PWM. A temperature sensor LM35 is used to measure the surface temperature of the battery, but it is not of significant value as the internal temperature rise is the variable sought after, which is calculated using (17). Using the measured current from the experimental setup, the SoC of the battery is estimated using following equation:

$$SOC(t) = SOC(t-1) + \frac{\int_{to}^{t} idt}{C_n}. \tag{24}$$

5.2. Driving Cycle

The experimental prototype is activated and the speed buttons are used to generate the driving cycle. Upon running the experiment, it is observed that the current rise happens at a very short interval. This is because no load is being applied to the shaft of the motor and the motor does not need to encounter any form of resistance. The motor picks up the inertia and keep running and the environmental resistance is negligible; hence, the current is very low. Therefore, a resistor is added to the circuit to observe a current flow in the circuit and to be able to run comparisons using stress equations illustrated in Chapter 3. The resistor added is around 2.5 Ohms to produce around 5 A of current. The proper wiring is used since a current of 5 A can cause overheating. The driving cycle in terms of the duty cycle of PWM gating signal of the DC/DC converter is described in Figure 5-3.

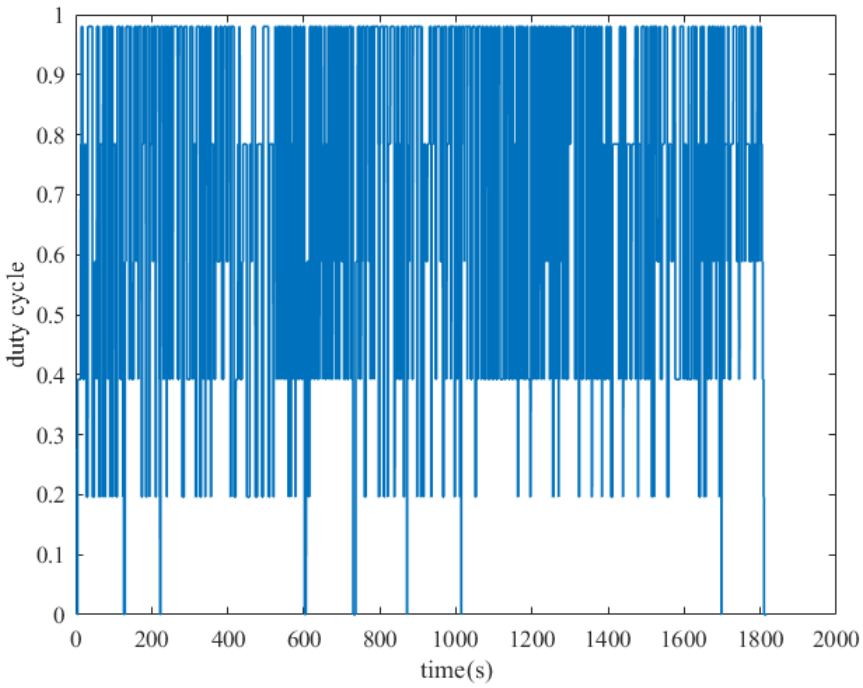

Figure 5-3: Duty cycle of gating PWM signal.

5.3. Experimental Results

The current supplied by the battery and SC in the HESS is shown in Figure 5-4. The same analysis used to evaluate the performance using simulation results is also carried out using the data obtained from the experiment. The method temperature and SoC are

calculated is illustrated in Section 3.5.1. The speed of the motors is obtained using LM393 optocoupler, as shown in Figure 5-5.

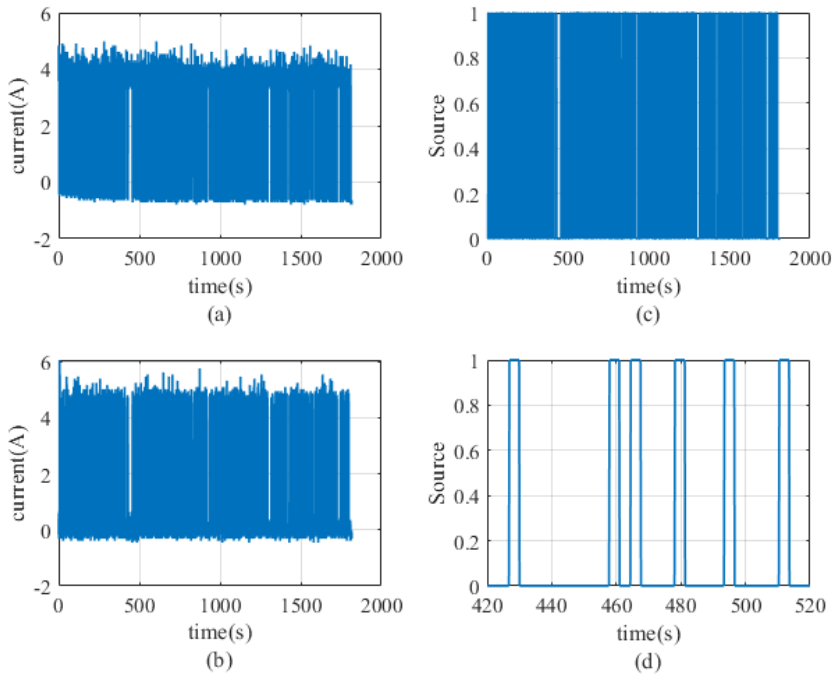

Figure 5-4: a) Battery's output current, b) SC output current, c) command signal from the processor to switch power source, d) command signal in small window of time.

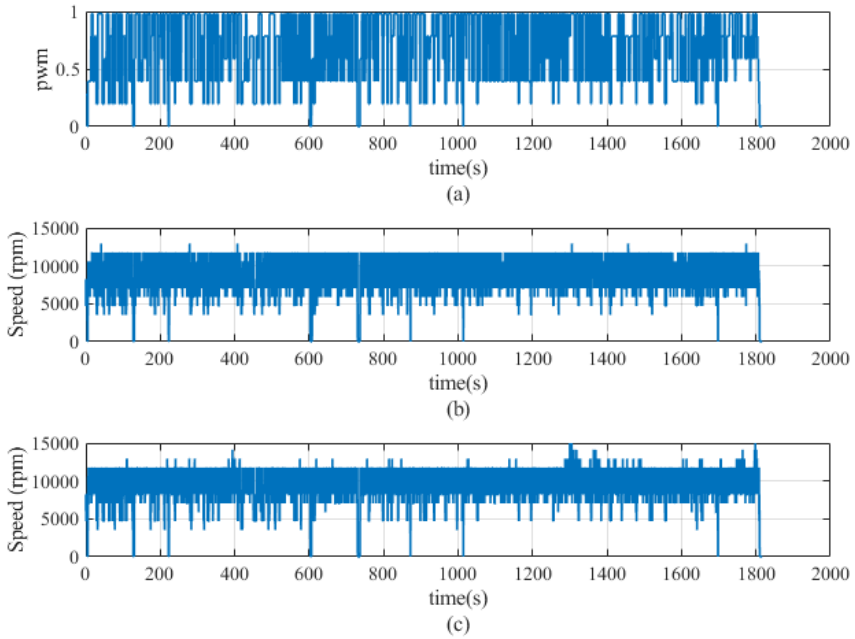

Figure 5-5: a) Duty cycle of PWM signal received by motor driver gates, b) speed of the motor in ESS, and c) speed of motor in HESS.

It should be noted that there is no closed loop system implemented to make sure both motors are running at the same speed. Nevertheless, the voltage is fixed at 12 V for all

sources and both motors are of the same model and the results show that they both run at almost the same speed; hence, the condition is even for both.

In Figure 5-4, the two figures on the left demonstrate the operation with the right bottom figure is a smaller window of the upper right figure. To deal with this experimentally, a command signal is sent to the processor to switch between the two sources. These two figures demonstrate the command signal to show an extra dimension in the circuit that was not present in the simulation. A low signal refers to battery powering up the circuit and high signal for the SC to operate. The negative current on the two figures on the right is error values produced by the current sensor which works on hall effect, and the performance of which can be altered by existing magnetic field or uncertainties. The battery output current in the traditional ESS is shown in Figure 5-6.

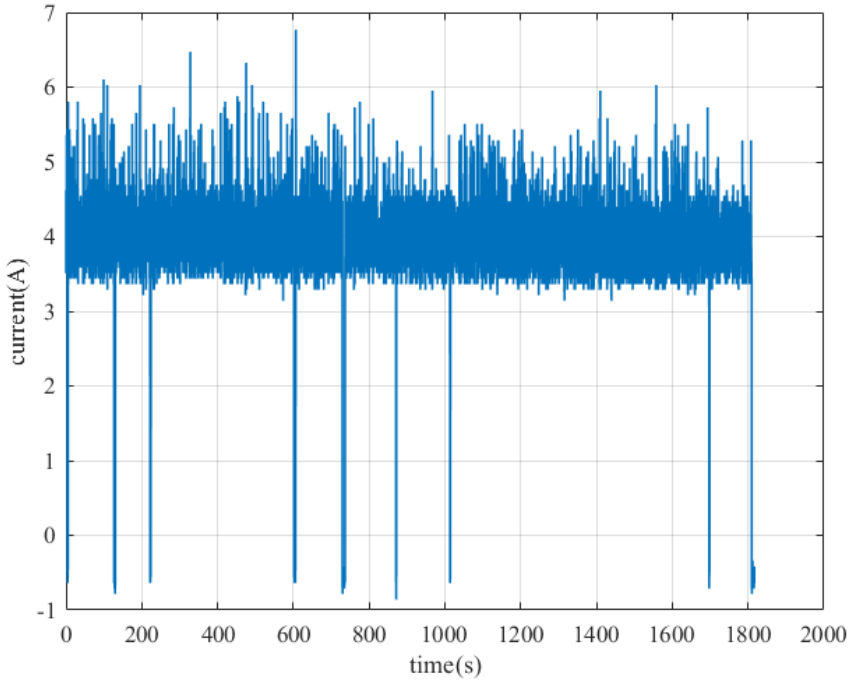

Figure 5-6: Battery's current output in ESS.

A comparison between the SoC levels of the EV battery in the HESS and the ESS is shown in Figure 5-7. By comparing the results in Figure 5-7(a) and (b), it is obvious that battery in HESS stores more charge at the end of the cycle compared to ESS. An additional loss of 10% in SOC of the battery in ESS takes place compared to HESS during the same driving cycle.

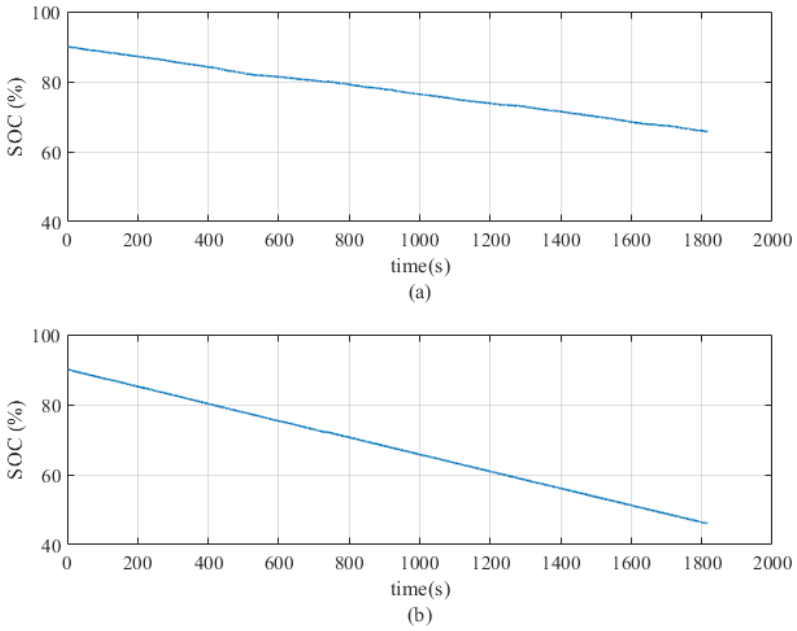

Figure 5-7: a) Battery's SOC level in HESS, b) battery's SOC level in traditional ESS.

Temperature sensor LM35 is mounted on the battery by taping it on the surface. The results obtained from the sensor is the surface temperature of the battery with no knowledge about the temperature rise inside the battery. The temperature recorded from the sensor fluctuates slightly around room temperature and no specific pattern is observed, which concludes that the fluctuations are basically sensor behavior. Therefore, using temperature sensor on the surface of the battery to record temperature is not a correct approach in this case as our batteries do not operate at a very high current for the temperature to be sensed at the surface and the rise of temperature internally is not sensed outside due to the insulations. Hence, to record the rise of temperature taking place inside the battery equation (17) is used, and the corresponding thermal stress is measured using (18). The equations take into consideration the variation of resistance due to temperature, and therefore are used.

5.4. Performance Evaluation

5.4.1 Thermal stress

The rise in temperature and corresponding thermal stress are shown in Figure 5-8 and Figure 5-9, respectively.

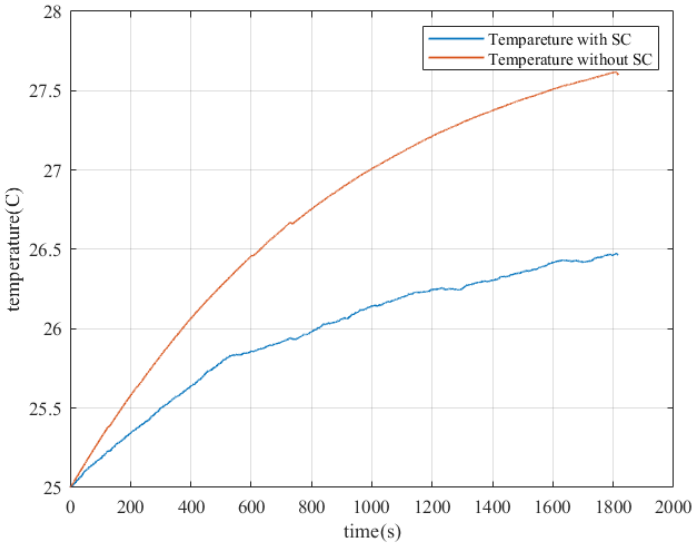

Figure 5-8: Battery's temperature rise in ESS and HESS.

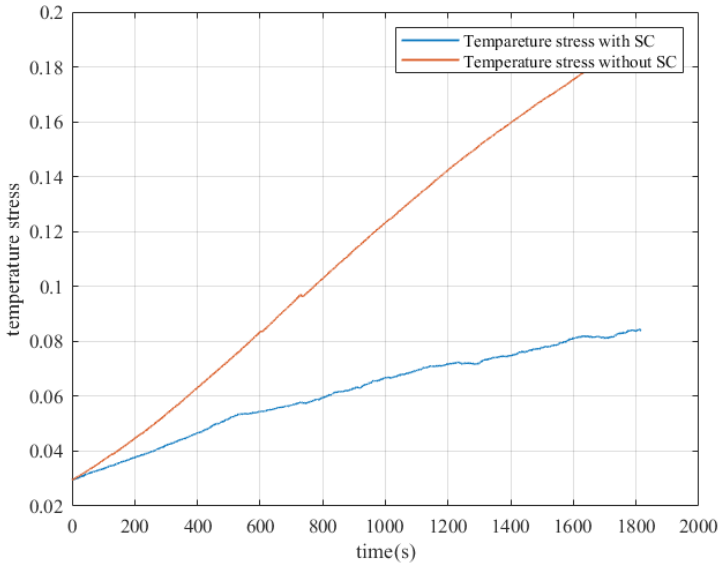

Figure 5-9: Thermal stress corresponding to temperature rise in HESS and ESS.

By comparing Figure 5-8 and Figure 5-9, to Figure 4-8 and Figure 4-9, and Figure 4-22 and Figure 4-23, the same enhancement in thermal performance of the EV battery is observed in the HESS when compared to the ESS. This verifies the accuracy of the simulation results and the reliability of the conducted experimental verification.

5.4.2 Time stress

Time stress obviously grows larger without SC as explained previously and is verified using the experimental data, as shown in Figure 5-10. Following the pattern observed

in simulation results, the plots in Figure 5-10 reveal that the time stress on battery in HESS is less compared to ESS.

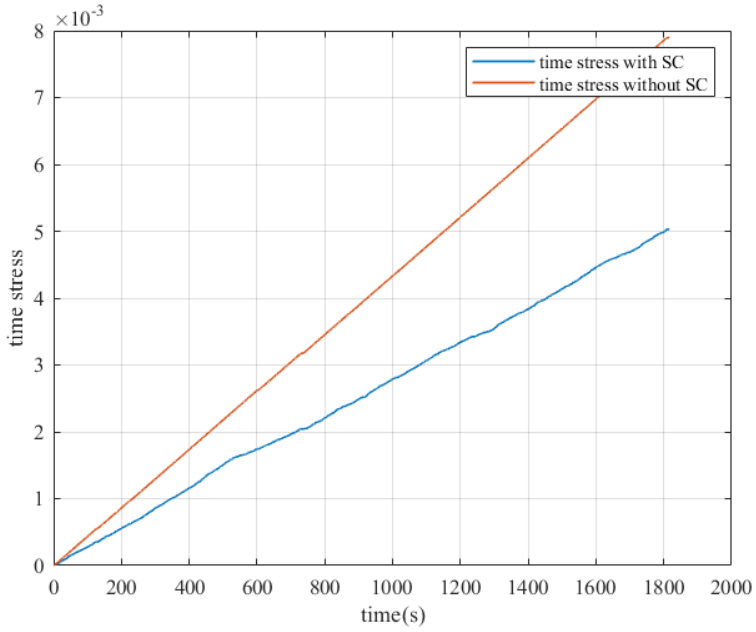

Figure 5-10: Time stress in HESS and ESS.

5.4.3 SoC stress

SoC stress on the EV battery in the ESS and the HESS is in Figure 5-11.

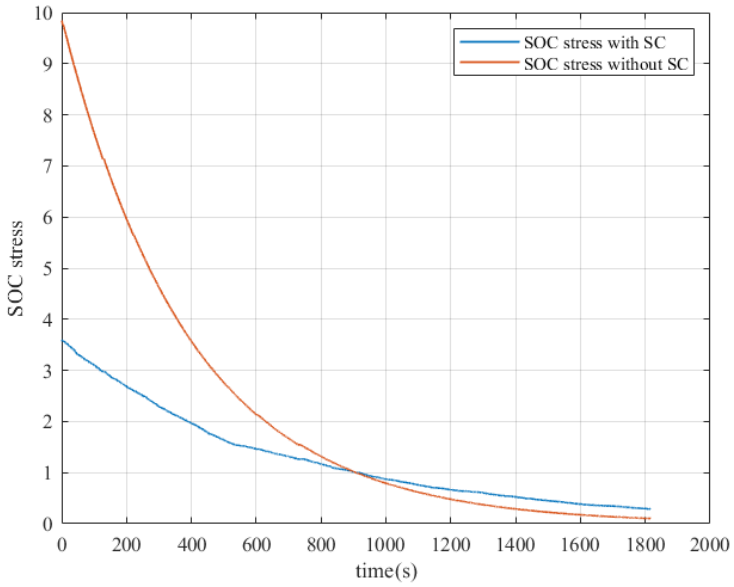

Figure 5-11: Battery's SoC stress in ESS and HESS.

An interesting pattern is observed in Figure 5-11, where more stress on the battery in ESS is observed at the beginning of the cycle and less stress is observed towards the end of the cycle. This is because the reference SoC in the SoC stress equation is taken to be the average SoC of the cycle.

5.4.4 Calendar aging and loss in capacity

The loss in capacity as a result of stress factors is demonstrated in Figure 5-12.

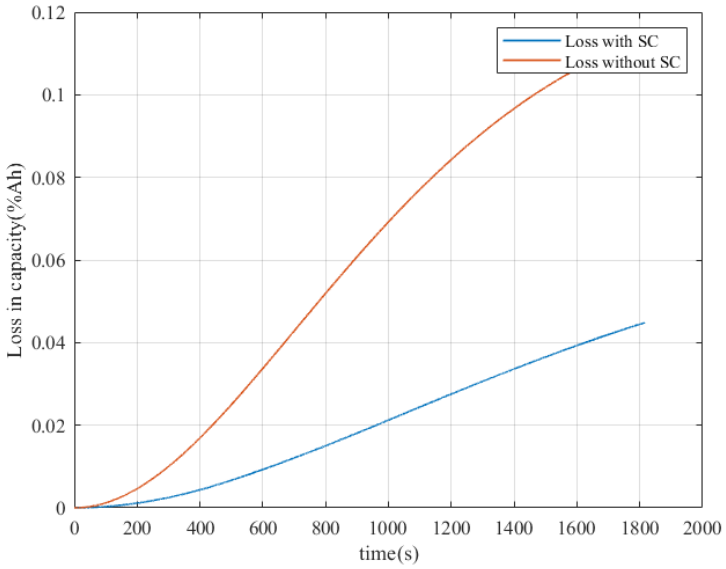

Figure 5-12: Percentage loss of capacity.

The experimental results show an improvement of 3 times by using HESS compared to ESS, which is still considered as a significant improvement.

5.5. Cost Justifications

It is important to run cost analysis to determine whether it is worth the investment or not. The analysis is done assuming that ZOXCELL SC model is used. The corresponding pricing details are shown in Table 5-2.

Table 5-2: SC bank price [65].

Item	ZOXCELL supercapacitor
Cost/cell	$ 4.08
Cost of the SC bank consisting of 400 SCs	$ 1632.00

An EV battery is expected to last for 8-10 years and costs $ 13,000 for replacement [66]. Theoretically if the battery lifetime can be extended by two times of its lifetime in ESS, then around $12,000 is saved for each replacement, and the investment is definitely profitable. However, according to the results, enhancement over two times is expected.

Chapter 6. Conclusion and Future Work

In essence, this thesis focuses on implementing a new energy management strategy to successfully integrate and operate supercapacitor bank in the energy storage system of electric vehicles and manage the energy flow of both battery and SC banks. This is vital as it aids in reducing battery aging and increasing the driving range of the EV, which are the two main issues concerning EV users. Two different circuits and energy flow control strategies have been proposed in this thesis. Both circuits are built on Simulink and the algorithm for each one is implemented to run the simulation. The results are obtained to evaluate stress factor and assess aging of both proposed methods and compare them against a traditional energy storage system consisting of only a battery powering the system. The results reveal five times improvement in battery aging performance, which is a notable improvement. For experimental verification, a circuit with a control algorithm that mimics the simulation at smaller scale is designed, which also resulted in a noticeable improvement of the HESS. The method adopted to deal with hybridization aims to be efficient and practical, which has been achieved. As for future work, an experiment involving higher battery ratings, power electronic devices and motors must be connected. Moreover, the improvement offered by the supercapacitor bank during wireless charging of EVs needs to be examined.

References

[1] I. T. Vadium, R. Das, Y. Wang, G. Putrus and R. Kotter, "Electric vehicle carbon footprint reduction via intelligent charging strategies," *2019 8th International Conference on Modern Power Systems (MPS)*, Cluj Napoca, Romania, 2019, pp. 1-6, doi: 10.1109/MPS.2019.8759783.

[2] E. A. Elghanam, M. S. Hassan, and A. Osman, “Design of a High Power, LCC-Compensated, Dynamic, Wireless Electric Vehicle Charging System with Improved Misalignment Tolerance,” *Energies*, 14, 2021, pp. 885. https://doi.org/10.3390/en14040885.

[3] A. O. el Meligy, E. A. Elghanam, M. S. Hassan and A. H. Osman, "Deployment Optimization of Dynamic Wireless Chargers for Electric Vehicles," 2021 *IEEE Transportation Electrification Conference & Expo (ITEC)*, 2021, pp. 113-118, doi: 10.1109/ITEC51675.2021.9490185.

[4] E. A. ElGhanam, M. S. Hassan and A. H. Osman, "Deployment Optimization of Dynamic Wireless Electric Vehicle Charging Systems: A Review," 2020 *IEEE International IOT, Electronics and Mechatronics Conference (IEMTRONICS)*, 2020, pp. 1-7, doi: 10.1109/IEMTRONICS51293.2020.9216415.

[5] Y. Louca, E. A. ElGhanam, M. S. Hassan and A. H. Osman, "Design and Modeling of Auxiliary Misalignment Detection Coils for Dynamic Wireless Electric Vehicle Charging Systems," 2021 *IEEE Transportation Electrification Conference & Expo (ITEC)*, 2021, pp. 125-129, doi: 10.1109/ITEC51675.2021.9490124.

[6] Fanning Jin, Mengqi Wang and Changjian Hu, "A fuzzy logic based power management strategy for hybrid energy storage system in hybrid electric vehicles considering battery degradation," *2016 IEEE Transportation Electrification Conference and Expo (ITEC)*, Dearborn, MI, 2016, pp. 1-7, doi: 10.1109/ITEC.2016.7520207.

[7] H. M. Sharf, E. A. ElGhanam, M. S. Hassan and A. H. Osman, "Assessing Efficiency and Aging of Lithium-Ion Battery in a Hybrid Energy Storage System," *2020 IEEE International IoT, Electronics and Mechatronics*

Conference (IEMTRONICS), Vancouver, BC, Canada, 2020, pp. 1-6, doi: 10.1109/IEMTRONICS51293.2020.9216426.

[8] H. M. Sharf, E. A. ElGhanam, M. S. Hassan, A. H. Osman and A. O. ElMeligy, "Performance Enhancement of a Hybrid Battery-Supercapacitor EV Energy Storage System," 2021 *IEEE Transportation Electrification Conference & Expo (ITEC)*, 2021, pp. 702-707, doi: 10.1109/ITEC51675.2021.9490063.

[9] N. Sato, "Thermal behavior analysis of lithium-ion batteries for electric and hybrid vehicles", *Journal of Power Sources*, vol. 99, no. 1-2, pp. 70-77, 2001. Available: 10.1016/s0378-7753(01)00478-5 [Accessed 2 February 2021].

[10] A. Gailani, R. Mokidm, M. El-Dalahmeh, M. El-Dalahmeh and M. Al-Greer, "Analysis of Lithium-ion Battery Cells Degradation Based on Different Manufacturers," *2020 55th International Universities Power Engineering Conference (UPEC)*, 2020, pp. 1-6, doi: 10.1109/UPEC49904.2020.9209759.

[11] X.-G. Yang, Y. Leng, G. Zhang, S. Ge, and C.-Y. Wang, "Modeling of lithium plating induced aging of lithium-ion batteries: Transition from linear to nonlinear aging," *Journal of Power Sources*, vol. 360, pp. 28- 40, 2017

[12] M. S. D. Darma et al., "The influence of cycling temperature and cycling rate on the phase specific degradation of a positive electrode in lithium ion batteries: A post mortem analysis," *Journal of Power Sources*, vol. 327, pp. 714-725, 2016.

[13] U. R. Koleti, T. Q. Dinh, and J. Marco, "A new on-line method for lithium plating detection in lithium-ion batteries," *Journal of Power Sources*, vol. 451, p. 227798, 2020.

[14] D. Stroe, M. Swierczynski, S. K. Kær and R. Teodorescu, "A comprehensive study on the degradation of lithium-ion batteries during calendar ageing: The internal resistance increase," 2016 *IEEE Energy Conversion Congress and Exposition (ECCE)*, 2016, pp. 1-7, doi: 10.1109/ECCE.2016.7854664.

[15] J. Vetter et al., "Ageing mechanisms in lithium-ion batteries," *J. Power Sources*, vol. 147, nos. 1–2, pp. 269–281, 2005. [Online]. Available: http://www.sciencedirect.com/science/article/pii/S0378775305000832

[16] Käbitz, M. Ecker, and D. U. Sauer, "Modeling mechanical degradation in lithium ion batteries during cycling: Solid electrolyte interphase fracture," *J. Power Sources*, vol. 300, pp. 112–122, Dec. 2015.

[17] J. Wang et al., “Cycle-life model for graphite-LiFePO4 cells,” *J. Power Sources*, vol. 196, no. 8, pp. 3942–3948, 2011

[18] A. Millner, “Modeling lithium ion battery degradation in electric vehicles,” in *Proc. IEEE Conf. Innov. Technol. Efficient Rel. Electricity Supply (CITRES)*, Waltham, MA, USA, 2010, pp. 349–356.

[19] M. Kassem et al., “Calendar aging of a graphite/LiFePO_4 cell,” *J. Power Sources*, vol. 208, pp. 296–305, 2012.

[20] B. Xu, A. Oudalov, A. Ulbig, G. Andersson and D. S. Kirschen, "Modeling of Lithium-Ion Battery Degradation for Cell Life Assessment," in *IEEE Transactions on Smart Grid*, vol. 9, no. 2, pp. 1131-1140, March 2018, doi: 10.1109/TSG.2016.2578950.

[21] Liu, Huijun & Chen, Fenfang & Tong, Yuxiang & Wang, Zihang & Yu, Xiaoli & Huang, Rui. (2020). Impacts of Driving Conditions on EV Battery Pack Life Cycle. World Electric Vehicle Journal. 11. 17. 10.3390/wevj11010017.

[22] N. Sato, "Thermal behavior analysis of lithium-ion batteries for electric and hybrid vehicles", *Journal of Power Sources*, vol. 99, no. 1-2, pp. 70-77, 2001. Available: 10.1016/s0378-7753(01)00478-5 [Accessed 2 February 2021].

[23] I. Baghdadi, O. Briat, J.-Y. Deletage, J.-M. Vinassa, and P. Gyan, “Dynamic battery aging model: Representation of reversible capacity losses using first order model approach,” 10 2015, pp. 1–4.

[24] R. Drummond, G. Valmorbida and S. Duncan, "Equivalent Circuits for Electrochemical Supercapacitor Models", *IFAC-PapersOnLine*, vol. 50, no. 1, pp. 2671-2676, 2017. Available: 10.1016/j.ifacol.2017.08.551 [Accessed 2 February 2021]

[25] P. J. Grbovic, P. Delarue, P. Le Moigne, and P. Bartholomeus, “Modeling and control of the ultracapacitor-based regenerative controlled electric drives,” *IEEE Transactions on Industrial Electronics*, vol. 58, no. 8, pp. 3471–3484, 2011.

[26] A. S. Weddell, G. V. Merrett, T. J. Kazmierski, and B. M. Al-Hashimi, “Accurate supercapacitor modeling for energy harvesting wireless sensor nodes,” *IEEE Transactions on Circuits and Systems II: Express Briefs*, vol. 58, no. 12, pp. 911–915, 2011.

[27] V. Musolino, L. Piegari, and E. Tironi, “New full-frequency-range supercapacitor model with easy identification procedure,” *IEEE Transactions on Industrial Electronics*, vol. 60, no. 1, pp. 112–120, 2013.

[28] N. Bertrand, J. Sabatier, O. Briat, and J. Vinassa, “Embedded fractional nonlinear supercapacitor model and its parametric estimation method,” *IEEE Transactions on Industrial Electronics*, vol. 57, no. 12, pp. 3991– 4000, 2010

[29] H. Gualous, R. Gallay, A. Crausaz, and A. Berthon, “Frequency, thermal and voltage supercapacitor characterization and modeling,” *Journal of Power Sources*, vol. 165, p. 928–934, 03 2007.

[30] Rengui Lu, Guoliang Wu, Rui Ma, and Chunbo Zhu, “Model based state of charge estimation method for ultra-capacitor,” in 2008 *IEEE Vehicle Power and Propulsion Conference*, 2008, pp. 1–5.

[31] A. Khaligh and Z. Li, “Battery, ultracapacitor, fuel cell, and hybrid energy storage systems for electric, hybrid electric, fuel cell, and plugin hybrid electric vehicles: State of the art,” *IEEE Transactions on Vehicular Technology*, vol. 59, no. 6, pp. 2806–2814, 2010.

[32] R. Kopka, "Estimation of Supercapacitor Energy Storage Based on Fractional Differential Equations", *Nanoscale Research Letters*, vol. 12, no. 1, 2017. Available: 10.1186/s11671-017-2396-y [Accessed 2 February 2021].

[33] S. M. Lukic, S. G. Wirasingha, F. Rodriguez, J. Cao, and A. Emadi, “Power management of an ultra-capacitor/battery hybrid energy storage system in an HEV,” in *Proc. IEEE Veh. Power Propulsion Conf.*, Windsor, U.K., Sep. 2006, pp. 1–6.

[34] M. Ortuzar, J. Moreno, and J. Dixon, “Ultracapacitor-based auxiliary energy system for an electric vehicle: Implementation and evaluation,” *IEEE Trans. Ind. Electron.*, vol. 54, no. 4, pp. 2147–2156, Aug. 2007.

[35] W. Lhomme, P. Delarue, P. Barrade, A. Bouscayrol, and A. Rufer, “Design and control of a supercapacitor storage system for traction applications,” in *Proc. Conf. Rec. Ind. Appl. Conf.*, Oct. 2005, pp. 2013–2020.

[36] X. Liu, Q. Zhang, and C. Zhu, “Design of battery and ultracapacitor multiple energy storage in hybrid electric vehicle,” in *2009 IEEE Vehicle Power and Propulsion Conference*, 2009, pp. 1395–1398.

[37] I. Azizi and H. Rajeai, “A new strategy for battery and supercapacitor energy management for an urban electric vehicle,” *Electrical Engineering*, 2017.

[38] H. Xiaoliang, H. Yoichi, and H. Tosiyoki, “Bidirectional power flow control for battery super capacitor hybrid energy system for electric vehicles with in-wheel motors,” in 2014 16th *International Power Electronics and Motion Control Conference and Exposition*, 2014, pp. 1078–1083.

[39] J. Cao and A. Emadi, "A New Battery/UltraCapacitor Hybrid Energy Storage System for Electric, Hybrid, and Plug-In Hybrid Electric Vehicles," in *IEEE Transactions on Power Electronics*, vol. 27, no. 1, pp. 122-132, Jan. 2012, doi: 10.1109/TPEL.2011.2151206.

[40] B. Nguyen, R. German, J. P. Trovao, and A. Bouscayrol, “Improved voltage limitation method of supercapacitors in electric vehicle applications,” in 2016 *IEEE Vehicle Power and Propulsion Conference* (VPPC), 2016, pp. 1–6.

[41] R. Carter, A. Cruden, and P. J. Hall, “Optimizing for efficiency or battery life in a battery/supercapacitor electric vehicle,” *IEEE Trans. Veh. Technol*., vol. 61, no. 4, pp. 1526–1533, May 2012.

[42] L. Sun, K. Feng, C. Chapman and N. Zhang, "An Adaptive Power-Split Strategy for Battery–Supercapacitor Powertrain—Design, Simulation, and Experiment," in *IEEE Transactions on Power Electronics*, vol. 32, no. 12, pp. 9364-9375, Dec. 2017, doi: 10.1109/TPEL.2017.2653842.

[43] A. Jaafar, C. R. Akli, B. Sareni, X. Roboam, and A. Jeunesse, “Sizing and energy management of a hybrid locomotive based on flywheel and accumulators,” *IEEE Trans. Veh. Technol*., vol. 58, no. 8, pp. 3947–3958, Oct. 2009.

[44] E. Schaltz, A. Khaligh, and P. O. Rasmussen, “Influence of battery/ultracapacitor energy-storage sizing on battery lifetime in a fuel cell hybrid electric vehicle,” *IEEE Trans. Veh. Technol*., vol. 58, no. 8, pp. 3882–3891, Oct. 2009.

[45] Vey, R. Roche, B. Blunier, and A. Miraoui, “Combined optimal sizing and energy management of hybrid electric vehicles,” in *Proc. Transp. Electrific. Conf. Expo*., Jun. 18–20, 2012, pp. 1–6.

[46] Z. Chenghui, S. Qingsheng, C. Naxin, and L. Wuhua, “Particle swarm optimization for energy management fuzzy controller design in dual-source

electric vehicle," *in Proc. Power Electron. Spec. Conf*., Jun. 17–21, 2007, pp. 1405–1410.

[47] H. F. Gharibeh, L. Mokhtari Khiavi, M. Farrokhifar, A. Alahyari and D. Pozo, "Power Management of Electric Vehicle Equipped with Battery and Supercapacitor Considering Irregular Terrain," *2019 International Youth Conference on Radio Electronics, Electrical and Power Engineering (REEPE)*, 2019, pp. 1-5, doi: 10.1109/REEPE.2019.8708770.

[48] L. Zhang, X. Xia, and F. Barzegar, "Control of a battery/supercapacitor hybrid energy storage system for electric vehicles," in 2017 36th Chinese Control Conference (CCC), 2017, pp. 9560–9565.

[49] K. Miettinen, *Nonlinear Multiobjective Optimization*, vol. 12. New York, NY, USA: Springer, 2012.

[50] F. Machado, J. P. F. Trovao, and C. H. Antunes, "Effectiveness of ˜ supercapacitors in pure electric vehicles using a hybrid metaheuristic approach," *IEEE Transactions on Vehicular Technology*, vol. 65, no. 1, pp. 29–36, 2016.

[51] Li and N. C. Kar, "Advanced design approach of power split device of plug-in hybrid electric vehicles using dynamic programming," in Proc. IEEE Veh. Power Propulsion Conf., Chicago, IL, USA, 2011, pp. 1–6.

[52] L. Zhang and D. G. Dorrell, "Genetic algorithm based optimal component sizing for an electric vehicle," in *Proc. 39th Annu. Conf. IEEE Ind. Electron. SoC.*, Vienna, Austria, 2013, pp. 7331–7336.

[53] G. Adinolfi, G. Graditi, P. Siano, and A. Piccolo, "Multiobjective optimal design of photovoltaic synchronous boost converters assessing efficiency, reliability, and cost savings*," IEEE Trans. Ind. Informat*., vol. 11, no. 5, pp. 1038–1048, Oct. 2015.

[54] J. Shen and A. Khaligh, "A supervisory energy management control strategy in a battery/ultracapacitor hybrid energy storage system," *IEEE Trans. Transp. Electrific.,* vol. 1, no. 3, pp. 223–231, Oct. 2015.

[55] Moreno, M. E. Ortuzar, and J. W. Dixon, "Energy-management system for a hybrid electric vehicle, using ultracapacitors and neural networks," *IEEE Trans. Ind. Electron*., vol. 53, no. 2, pp. 614–623, Apr. 2006.

[56] Z. Liang, Z. Xin, T. Yi, and Z. Xinn, “Intelligent energy management for parallel HEV based on driving cycle identification using SVM,” in *Proc. 2nd Int. Symp. Comput. Intell. Des*., 2009, 513–516.

[57] R. Langari and W. Jong-Seob, “Intelligent energy management agent for a parallel hybrid vehicle—Part I: System architecture and design of the driving situation identification process,” *IEEE Transactions on Vehicular Technol*ogy, vol. 54, no. 3, pp. 925–934, May 2005.

[58] Di Silvestre et al., “An optimization approach for efficient management of EV parking lots with batteries recharging facilities,” *J. Ambient Intell. Humanized Comput*., vol. 4, no. 6, pp. 641–649, 2013.

[59] Q. Gong, Y. Li, and Z. R. Peng, “Trip-based optimal power management of plug-in hybrid electric vehicles,” *IEEE Transactions on Vehicular Technol*ogy, vol. 57, no. 6, pp. 3393–3401, Nov. 2008.

[60] . Wikner and T. Thiringer. “Extending Battery Lifetime by Avoiding High SOC,” *Applied Sciences, 8,* 1825, 2018. https://doi.org/10.3390/app8101825

[61] S. S. Choi and H. S. Lim, “Factors that affect cycle-life and possible degradation mechanisms of a li-ion cell based on LiCoO2,” *J. Power Sources*, vol. 111, no. 1, pp. 130–136, 2002.

[62] P. Novák et al., “The complex electrochemistry of graphite electrodes in lithium-ion batteries,” *J. Power Sources*, vols. 97–98, pp. 39–46, Jul. 2001.

[63] J. Li, E. Murphy, J. Winnick, and P. A. Kohl, “The effects of pulse charging on cycling characteristics of commercial lithium-ion batteries,” *J. Power Sources*, vol. 102, nos. 1–2, pp. 302–309, 2001.

[64] Dynamometer drive schedules, Aug. 20, 2016. [Online]. Available: https://www.epa.gov/vehicle-and-fuel-emissions-testing/dynamometerdrive-schedule

[65] Zoxcell | Graphene Supercapacitor Battery & Energy Storage Solution Manufacturer", Zoxcell.com, 2021. [Online]. Available: https://www.zoxcell.com/?gclid=CjwKCAiA1aiMBhAUEiwACw25Mco7d00LLFCU5ItBU5OQVjDWWIDoeWH_bP02tvg6rPsOFNEwfoSMRoCe5AQAvD_BwE. [Accessed: 09- Nov- 2021].

[66] Will worn-out batteries send Tesla to the scrapheap? It's complicated", Inverse, 2021. [Online]. Available: https://www.inverse.com/innovation/tesla-battery-life-replacement-cost. [Accessed: 09- Nov- 2021].

Vita

Hazem Magdi Sharf was born in 1997, in Al Ain city, Abu Dhabi, United Arab Emirates. He received his primary and secondary education in Al Ain, and received his B.Sc. degree in Electrical Engineering from the American University of Sharjah in 2019.

In September 2019, he joined the Electrical Engineering Master's program in the American University of Sharjah as a graduate teaching and research assistant. During his master's study, he co-authored 2 papers which were presented at international conferences. His research interests are in electronics, control and circuit design, and electrified transportation systems.